http://dx.doi.org/10.1016/j.ijplas.2016.11.011

Constitutive modeling of size effect on deformation behaviors of elasto-viscoplastic polymers in micro-scaled deformation

Y.J. Deng [a, b], L.F. Peng [a], X.M. Lai [a*], M.W. Fu [b**], Z.Q. Lin[a]

[a] State Key Laboratory of Mechanical System and Vibration, Shanghai Jiao Tong University, Shanghai 200240, People's Republic of China

[b] Department of Mechanical Engineering, The Hong Kong Polytechnic University, Hung Hom, Kowloon, Hong Kong

* Corresponding authors:

* Tel.: +8602134206303. E-mail address: xmlai@sjtu.edu.cn (X.M. Lai).

** Tel.: +852-27665527. E-mail address: mmmwfu@polyu.edu.hk (M.W. Fu).

Abstract:

With the advantages of high-formability, low-cost and unique physical properties, polymers have been widely used in microforming of polymeric components for a large scale of applications in many fields including micro-optics, microfluidic and sensors, etc. In micro-scale, the deformation behaviors of polymers are observed to be size-dependent. Conventional constitutive models of polymers, however, cannot predict and represent those size-dependent behaviors well. To address this issue, a constitutive model with consideration of size effect for amorphous polymers in the micro-scale was developed in this research. Firstly, on the basis of the couple stress theory, the impact of rotational gradients was taken into consideration and a strain gradient elasto-viscoplastic constitutive model was proposed to quantitatively describe the size-dependent behaviors of amorphous polymers in micro-scale. After that, four-point micro-bending experiments were implemented on poly (methyl methacrylate) (PMMA) plates with thickness varying from the millimeter scale to

micrometer scale. The size effect of PMMA in micro-scale was further illustrated and the proposed strain gradient elasto-viscoplastic model was lastly validated and verified for the capability of modeling of the size effect of amorphous polymers in micro deformations. This research thus advances the understanding of the size effect and the strain gradient based mechanical behaviors of amorphous polymers and facilitates its applications in industries.

Keywords:

Strain gradient theory; A. Size effect; B. Amorphous polymer; B. Constitutive behavior; B. Elasto-viscoplastic material

1. Introduction

Product miniaturization and multi-functional integration significantly increase the demand for micro-scaled parts and components. With the advantages of high-formability, low-cost and unique physical properties, polymeric materials have been widely used in forming of micro-scaled components including micro-optics, microfluidic, sensors, etc. To efficiently and accurately fabricate those micro-scaled polymeric parts, the mechanical behavior in micro-scaled deformation is one of the most significant issues to be explored and in-depth understanding of those behaviors is of great necessity to be established.

In micro-scale deformation, however, the mechanical responses of polymers have been observed to be size-dependent, which are different from those behaviors in macro-scale (Alisafaei et al., 2013; Alisafaei et al., 2014; Díez-Pascual et al., 2015; Han et al., 2016; Shirazi et al., 2016; Tjernlund et al., 2004; Wrucke et al., 2013). To name a few, Briscoe et al. (1998) observed that both the hardness and Young's modulus of poly(styrene) (PS), poly(methylmethacrylate) (PMMA) and poly(carbonate) (PC) tended to increase when the

depth decreased to 1 μm. Similarly, Chong et al. (1999) reported that both thermosetting epoxy and PC had the constant hardness at large indentation depth but exhibited hardening when the depth was smaller than 1.5 μm. After that, Tatiraju et al. (2008) demonstrated an increase of 70% in hardness of polyamide/imide (PAI) when the penetrating depth of nanoindentation decreased from 30 to 1 μm. He et al. (2008) performed diametric compression experiments on micron-sized spheres of polystyrene-divenylbenzene (PS-DVB) and observed that the stress at 4% strain increases by almost 50% as the diameter of the spheres decrease from 25 to 2.5 μm. Recently, Wang et al. (2012) reported significant increase in yield and fracture strength with decrease in diameter of epoxy pillars from about 5 μm to sub-micron ranges. Moreover, the size effect of polymers has also been observed in micro-bending experiments. Initially, Lam et al. (2003) demonstrated that the elastic bending rigidity of epoxy cantilever beams increased by about 2.4 times when the beam thickness reduced from 115 to 20 μm. Later, McFarland and Colton (2005) found that the measured stiffness of polypropylene (PP) beams with the thickness of about 15 μm was at least four times higher than the predicted stiffness by classical continuum theory. Additionally, Lam et al. (2010) further illustrated that the creep deflection behavior of epoxy beams followed the conventional Kelvin-Voigt viscoelastic behavior when the beams were thick and that higher-order size dependences were present in both the time-independent elastic and time-dependent creep deflection when the beams were thin.

Actually, the size effect has been observed in the micro forming of metallic materials (Fu and Chan, 2011; Meng and Fu, 2015; Peng et al., 2009; Ran et al., 2013; Xu et al., 2015). Notably for metallic materials, the size effect on the elastic deformation is usually ignored

and the studies on the size effect are mainly concentrated on the size-dependent plastic deformation behaviors in micro-scale. For polymeric materials, however, the elastic strain takes up a significant proportion and plays a big role in deformation, which is thus needed to be considered in the classical constitutive models such as viscoelasticity (e.g., Deng et al., 2015, Wang et al., 2015), viscoelastic-plasticity (e.g., Drozdov, 2010; Menčík et al., 2011), elasto-viscoplasticity (e.g., Anand et al., 2012, Lebensohn et al., 2012, Poulain et al., 2014, Zaïri et al., 2008, Zhang and To, 2016) and viscoelastic-viscoplasticity (e.g., Abdul-Hameed et al., 2014, Haouala and Doghri, 2015, Yoon and Huang, 2011) based models. In this way, when the feature size of forming decreases into micro-scale, the size-dependent elasticity of amorphous polymers should be considered at the same time. In the past few decades, prior efforts have been made to represent the size effect of polymers separately from the aspect of size-dependent elasticity and size-dependent plasticity, on the basis of the strain gradient theory.

On the one hand, from the aspect of the size-dependent elasticity, Lam et al. (2003) initially developed a new set of higher-order metrics to characterize strain gradient elasticity and found that the higher-order bending solutions have a good agreement with the measured size-dependent stiffness of epoxy beams. After that, McFarland and Colton (2005) proposed a model based upon a micropolar elasticity constitutive model to represent the increasing bending stiffness with the decrease of the cantilever thickness and Park and Gao (2006) developed a bending model for the Bernoulli-Euler beam based on a modified couple stress theory to describe the size effect of epoxy beam. Different from the phenomenon higher-order elastic model, Nikolov et al. (2007) related the energy contribution from rotational gradient to an effective Frank elastic constant to describe the size dependent elasticity of amorphous polymers. Moreover, Lam et al. (2010) further developed a higher

order viscoelasticity framework to describe the size effect of Maxwell and Kelvin-Voigt polymers. Ghosh et al. (2013) presented a molecular dynamics approach to model non-local elastic behaviors of epoxy using an atomistically-informed kernel. Recently, Alisafaei et al. (2016) expanded the above strain gradient elastic model (Nikolov et al., 2007) to represent the size effect in glassy polymer with elasto-plastic deformation and claimed that size effects in polymer were mainly of elastic nature even when glassy polymers deformed elasto-plastically.

On the other hand, from the plastic deformation perspective, Lam and Chong (1999) claimed that the statistically random kink pairs of glassy polymers were formed along with the geometrically necessary kink pairs when the material was subject to yield condition and the strain gradient. By introducing the strain gradient into the yielding model, they established a model to represent the hardness and indentation depth response of polymers and proposed a strain gradient plasticity modulus with temperature and molecular dependence. Later, Swaddiwudhipong et al. (2005) incorporated the effects of strain gradient plasticity developed by Lam and Chong (1999) to model size effect of glassy polymers in indentation using finite elements. Recently, Voyiadjis et al. (2014) developed a rate dependent plasticity theory with the strain gradient effect to represent the microscale mechanical response of semicrystalline polymers. It was concluded that the material length scale has a correlation with the microstructure of the polymer network as well as the course of deformation.

Existing theories for size effect of polymeric materials, while capable of predicting size-dependent elasticity and size-dependent plasticity separately, do not focus on the size-dependent plasticity at large deformation on the one hand and do not provide a complete constitutive model describing the size effect on both elasticity and plasticity simultaneously

on the other. Actually, in micro forming process, polymers usually experience a rather large strain before the microstructure is fabricated and the size effect on both the elasticity and plasticity happens at the same time. For this problem, the present research is focused on the development of a constitutive model for amorphous polymers which can handle both size-dependent elasticity and plasticity in micro-scale. The goal of this research is to provide an in-depth and panoramic understanding of the size-dependent deformation of amorphous polymers in such a way to provide systematic knowledge to support product design and quality control in micro-scaled polymeric components development.

2. Research procedure

The research procedure is summarized in Fig. 1. On the basis of the couple stress theory, the strain gradient elasto-viscoplastic constitutive model was firstly developed with the consideration of the impacts of the rotational gradient, for the purpose of quantitative prediction and description of the size effect of amorphous polymers in micro-scale. After that, four-point micro-bending experiments were designed and conducted on PMMA plates with thickness varying from the millimeter scale to micrometer scale. Based on the micro-bending results, the size effect of PMMA in micro-scale was further demonstrated and the intrinsic material lengths were calibrated for PMMA. Lastly, the strain gradient elasto-viscoplastic model was validated and verified for the ability of representation of the size-dependent behaviors of amorphous polymers in micron scale.

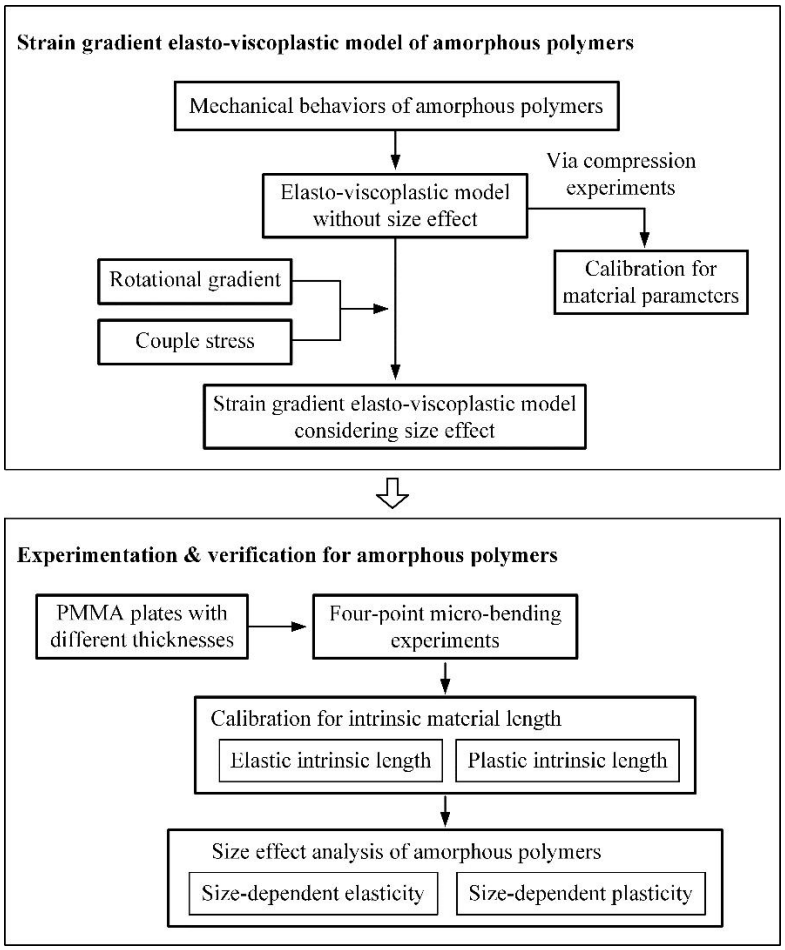

Fig. 1. Research procedure.

3. Strain gradient elasto-viscoplastic constitutive model of amorphous polymers

3.1 Elastic-viscoplastic behaviors

For the majority of amorphous polymers, with the increase of strain, the stress-strain response under a constant strain rate and a constant temperature below the glass transition temperature generally exhibits a linear elastic deformation and then strain softening after yield due to the near adiabatic heating at higher strain rate, and finally a steep hardening for the alignment and locking of molecular chains. In order to represent the mechanical behaviors of amorphous polymers in macro-scale, a quantitative description is proposed with a linear elastic part and a viscoplastic part connected in series, as shown in Fig. 2. By definition, the linear elastic part consists of a spring to model the linear elastic deformation of amorphous

polymers while the viscoplastic part combines a dashpot with the viscoplastic behavior and a spring with the nonlinear elastic behavior in parallel connection. Due to the parallel connection in the viscoplastic part, the dashpot and the spring have the same strain but different stresses. Hence, the total strain of this part mainly depends on the dashpot with viscoplastic and unrecoverable deformation and the contribution of the nonlinear spring is the increase of the stress especially for the case of large deformations for amorphous polymers.

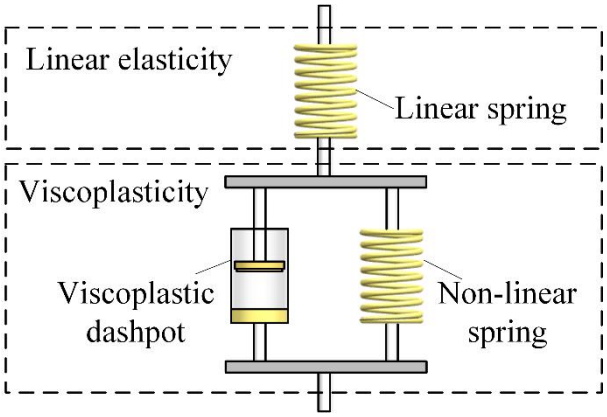

Fig. 2. Schematic of the elasto-viscoplastic behavior of amorphous polymers.

By definition, the overall strain is ε_{ij} and the overall stress is σ_{ij}. The strain is decomposed into the deviator strain e_{ij} and the volume strain ε_m in the following:

$$e_{ij} = \varepsilon_{ij} - \varepsilon_m \delta_{ij}, \tag{1}$$

where the volume strain $\varepsilon_m = \frac{1}{3}\varepsilon_{ii}$. The deviator strain e_{ij} is further decomposed into the elastic part e_{ij}^e related to the linear spring, and the viscoplastic part e_{ij}^p concerned with the combination of the viscoplastic dashpot and the non-linear spring.

Similarly, the stress is decomposed into the deviator stress S_{ij} and the hydrostatic pressure σ_m as:

$$S_{ij} = \sigma_{ij} - \sigma_m \delta_{ij}, \tag{2}$$

where the hydrostatic pressure $\sigma_m = \frac{1}{3}\sigma_{ii}$. On the basis of the assumption that the material volume is incompressible in plastic deformation, the hydrostatic pressure σ_m is related to the volume strain ε_m with the linear elastic behaviors as follows,

$$\sigma_m = \frac{E}{1-2\nu}\varepsilon_m, \tag{3}$$

where E is the Young's modulus, ν is the Poisson's ratio. Because the linear elastic and the viscoplastic part have the same stress components, the deviator stress S_{ij} can be obtained from the elastic strain of the Hookean spring e_{ij}^e through the following relation,

$$S_{ij} = \frac{E}{1+\nu}e_{ij}^e. \tag{4}$$

For the plastic deformation of amorphous polymers, Ree and Eyring (1995) claimed that yielding of amorphous polymers is achieved by surmounting the activation energy barrier for sliding of segments of macromolecular chain over others. Based on this rationale, they developed the famous model to describe the variation of yield stress with temperature and rate for amorphous polymers. In this work, the dashpot among the viscoplastic part is represented by the Eyring model to describe the rate-dependent plastic deformation of polymers. Based on the Eyring model, the effective plastic strain rate $\dot{\bar{e}}^p$ is formulated as,

$$\dot{\bar{e}}^p = \dot{\varepsilon}_0 \exp\left(-\frac{\Delta H}{k_B \vartheta}\right)\left[\sinh\left(\frac{\bar{\sigma}V}{2k_B\vartheta}\right)\right]^{1/m}, \tag{5}$$

where the effective plastic strain rate $\dot{\bar{e}}^p = \sqrt{\frac{2}{3}\dot{e}_{ij}^p\dot{e}_{ij}^p}$, and the effective shear stress $\bar{\sigma}$ is defined as $\bar{\sigma} \overset{def}{=} \sigma_{flow} - s$, σ_{flow} is the flow stress in Eyring dashpot, s is the internal variable (to be defined later), ϑ is the temperature, $\dot{\varepsilon}_0$ is a factor with unit of 1/time, ΔH is the activation energy, k_B is the Boltzman's constant, V is the shear activation volume,

and m is the strain rate sensitivity parameter.

For the nonlinear spring, in order to describe the strain hardening of polymers, the mechanical response of this spring is represented by the Langevin rubber model of which the stress of this spring increase non-linearly and rapidly when the strain get close to the limited elastic extensibility. Based on the langevin model by Treloar (1975) and Spathis and Kontou (2004), the stress in the nonlinear spring is giving by

$$\sigma_{back} = C_R \frac{\sqrt{n}}{3}\left[L^{-1}\left(\frac{1+\tilde{e}^p}{\sqrt{n}}\right) - \left(1+\tilde{e}^p\right)^{3/2} L^{-1}\left(\frac{1}{\left(1+\tilde{e}^p\right)^{1/2}\sqrt{n}}\right)\right], \tag{6}$$

where the function L^{-1} is the inverse function of Langevin function, $L(x) = \coth(x) - \frac{1}{x}$, $\left(n^{1/2}-1\right)$ corresponds to the limiting network strain, C_R is the rubber modulus, and $\tilde{e}^p = \sqrt{\frac{2}{3} e_{ij}^p e_{ij}^p}$ is the effective plastic strain.

Therefore, for the whole viscoplastic part, the effective stress $\tilde{S}$ is the sum of the dashpot stress σ_{flow} and the non-linear spring stress σ_{back}, as

$$\tilde{S} = \sigma_{flow} + \sigma_{back}, \tag{7}$$

where the effective stress is determined by $\tilde{S} = \sqrt{\frac{3}{2} S_{ij} S_{ij}}$.

Moreover, in order to describe the strain softening phenomenon after yielding, the internal variable s is introduced into viscoplastic part of the elasto-viscoplastic model. Referring to the definition of the internal variables by Anand et al. (2009), the internal variable s has the dimension of stress and represents an isotropic resistance to plastic flow and is coupled with a dimensionless parameter φ representing the local free-volume of polymeric glass, as

$$\begin{cases} \dot{\varphi} = g\left(\varphi^* - \varphi\right)\dot{\bar{e}}^p, & \varphi(0) = \varphi_i > 0 \\ \dot{s} = p\left(s^* - s\right)\dot{\bar{e}}^p, & s(0) = s_i \geq 0 \\ s^* = s_i + q\left(\varphi^* - \varphi\right) \end{cases}, \tag{8}$$

where the temperature and rate-dependence of p and q are described as the following particular functions,

$$\begin{cases} p = p_1 + p_2\vartheta \\ q = q_1\left(\vartheta^2 + q_2\vartheta + q_3\right)\left(\dfrac{\dot{\bar{e}}^p}{\dot{\varepsilon}_{ref}}\right)^{q_4} \end{cases}, \tag{9}$$

and $\{p_1, p_2, q_1, q_2, q_3, q_4\}$ are material parameters and $\dot{\varepsilon}_{ref}$ is a reference strain-rate.

Up to this point, the elasto-viscoplastic behaviors of amorphous polymers in macro-scale including linear elastic deformation, yielding, strain softening and strain hardening can all be described quantitatively by the integration of Eqs. (1) to (9).

In addition, uniaxial compression tests were conducted in this research to calibrate material parameters of the amorphous polymers. PMMA materials with excellent formability and wide applications in industry, were selected as an example to study the elasto-viscoplastic behaviors of the amorphous polymers. Commercial basic PMMA granules (Evonik Corporation Plexiglas 7N PMMA) were used for compression molding of plates and PMMA plates were then machined into cylindrical samples with the diameter of 6 mm and the height of 9 mm. Lastly, compression samples were annealed more than 12 h to minimize the residual stress. A servo-hydraulic Insrton testing machine with the load cell capacity of 10 kN was utilized. The true stress-strain curves of PMMA under different strain rates (0.0003, 0.0005, 0.001, 0.005, 0.01 and 0.05 s^{-1}) are shown in Fig. 3 by symbols.

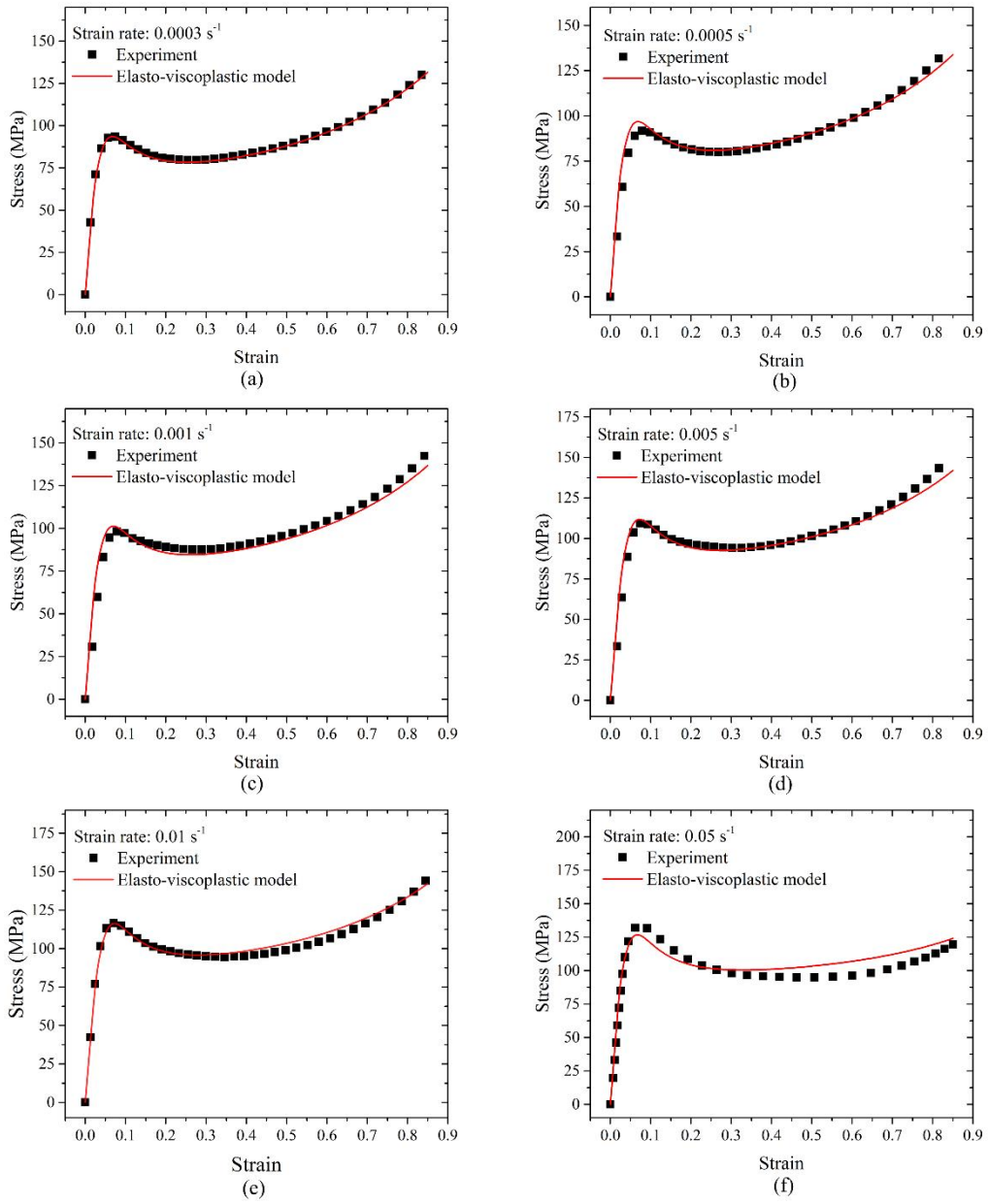

Fig. 3. True strain-stress curves of PMMA at the strain rate of (a) 0.0003 s^{-1}, (b) 0.0005 s^{-1}, (c) 0.001 s^{-1}, (d) 0.005 s^{-1}, (e) 0.01 s^{-1} and (f) 0.05 s^{-1}.

For the good description of the stress-strain response of amorphous polymers, the elastic moduli are determined as rate-dependent parameters, referring to the constitutive model of amorphous polymers proposed by Ames et al. (2009) and Srivastava et al. (2010). Particularly, Ames et al. (2009) specified the empirical function to fit the experimentally-observed temperature dependence of the elastic moduli of polymers and Srivastava et al. (2010) also

determined a temperature variation of the moduli to fit experimental trend of polymers instead of those dictated by statistical mechanic theories of entropic elasticity since the Gent free-energy function was also phenomenological. In the present work, the elastic moduli is also specified with empirical function to fit the experimentally-observed rate dependence, on the basis of the time-temperature equivalence principle of polymers.

According to the experimentally observed trends from the true stress-strain data of the PMMA, the elastic and rubbery moduli are assumed to be linearly dependent on the strain rate in this research. The change of the elastic modulus in Eq. (3) with the strain rate is given by

$$E = E^{ref} + X_E \dot{\bar{\varepsilon}}, \tag{10}$$

where E^{ref} is the reference Young's modulus and X_E describes the variation of the modulus with the strain rate. The modulus of the non-linear spring of viscoplastic part in Eq. (6) is designated as

$$C_R = C_R^{ref} - X_C \dot{\bar{\varepsilon}}, \tag{11}$$

where C_R^{ref} is the reference rubber modulus, and X_C is the parameter representing the slope of strain rate variation. In this way, the elasto-viscoplastic model of amorphous polymers at room temperature may be summarized as follows:

1）The relationships for the linear elastic part are

$$\begin{cases} S_{ij} = \dfrac{E}{1+\nu} e_{ij}^{e}, \\ \sigma_m = \dfrac{E}{1-2\nu} \varepsilon_m, \\ E = E^{ref} + X_E \dot{\bar{\varepsilon}}. \end{cases} \tag{12}$$

2）The relationships for the viscoplastic part are

$$\begin{cases} \tilde{S}=\sigma_{flow}+\sigma_{back}, \\ \dot{\tilde{e}}^{p}=\dot{\varepsilon}_{0}\exp\left(-\dfrac{\Delta H}{k_{B}\vartheta}\right)\left[\sinh\left(\dfrac{\bar{\sigma}V}{2k_{B}\vartheta}\right)\right]^{1/m}, \\ \bar{\sigma}=\sigma_{flow}-s, \\ \sigma_{back}=C_{R}\dfrac{\sqrt{n}}{3}\left[L^{-1}\left(\dfrac{1+\tilde{e}^{p}}{\sqrt{n}}\right)-\left(1+\tilde{e}^{p}\right)^{3/2}L^{-1}\left(\dfrac{1}{\left(1+\tilde{e}^{p}\right)^{1/2}\sqrt{n}}\right)\right], \\ C_{R}=C_{R}^{ref}-X_{C}\dot{\tilde{\varepsilon}}. \end{cases} \tag{13}$$

3）Internal variables are

$$\begin{cases} \dot{\varphi}=g\left(\varphi^{*}-\varphi\right)\dot{\tilde{e}}^{p},\varphi\left(0\right)=\varphi_{i}>0, \\ \dot{s}=p\left(s^{*}-s\right)\dot{\tilde{e}}^{p},s\left(0\right)=s_{i}\geq 0, \\ s^{*}=s_{i}+q\left(\varphi^{*}-\varphi\right), \\ q=q_{1}\left(\dfrac{\dot{\tilde{e}}^{p}}{\dot{\varepsilon}_{ref}}\right)^{q_{2}}. \end{cases} \tag{14}$$

To complete this model (Eqs. (12) to (14)) of a particular amorphous polymer, the material parameters to be determined include

$$\left\{E_{ref},X_{E},\Delta H,m,\dot{\varepsilon}_{0},V,C_{R}^{ref},X_{C},n,g,q_{1},q_{2},\dot{\varepsilon}_{ref},p\right\}.$$

With the help of commercial software MATLAB code, material parameters for PMMA were determined, as displayed in Table 1. Correspondingly, the predicted stress-strain data are also shown in Fig. 3 by solid lines. It is observed that the elasto-viscoplastic behaviors of PMMA materials in macro-scale are represented well.

Table 1

Material parameters of elasto-viscoplastic model for PMMA materials

Parameters	Value
E_{ref} (MPa)	2901

X_E (MPa·s)	1.79×10^{4}
ΔH (kJ mol^{-1})	109
m	0.548
$\dot{\varepsilon}_0$ (s^{-1})	1.51×10^{10}
V (mm^3)	9×10^{-19}
C_R^{ref} (MPa)	44.81
X_C (MPa·s)	492.34
n	5.57
g	11.8
q_1 (MPa)	3.6×10^{4}
q_2	0.0555
$\dot{\varepsilon}^{ref}$ (s^{-1})	3.0×10^{-4}
p (s)	78
ν	0.35

3.2 Strain gradient elasto-viscoplastic modeling

Previous works by Nikolov et al. (2007) and Wei and Lam (2010) illustrated that the effect of the rotational gradient as one of the strain gradients plays an important role in the mechanical behaviors of polymers in micro-scale. In this section, the impacts of the rotational gradient are introduced into the proposed elasto-viscoplastic model on the basis of the couple stress theory, to model the size effect of amorphous polymers in micro-scale.

According to the couple stress theory (Yang et al., 2002), the displacement gradient tensor $u_{i,j}$ is decomposed into the symmetric tensor ε_{ij} and the antisymmetric tensor ω_{ij} and

designated as:

$$u_{i,j} = \varepsilon_{ij} + \omega_{ij}, \tag{15}$$

$$\varepsilon_{ij} = \frac{1}{2}\left(u_{i,j} + u_{j,i}\right), \tag{16}$$

$$\omega_{ij} = \frac{1}{2}\left(u_{i,j} - u_{j,i}\right), \tag{17}$$

The rotation vector θ_i is determined as

$$\theta_i = -\frac{1}{2} e_{ijk}\omega_{jk}, \tag{18}$$

where e_{ijk} is the permutation symbol. An second-order tensor χ_{ij} was defined as the gradient of the rotation vector θ_i and was named as rotational gradient which can be written as

$$\boldsymbol{\chi} = \boldsymbol{\theta}\nabla, \quad \chi_{ij} = \theta_{i,j}. \tag{19}$$

An higher-order stress m_{ij} is work-conjugated with the rotational gradient χ_{ij} and is named as the couple stress. With the presence of the couple stress m_{ij}, Cauchy stress t_{ij} is not a symmetric tensor. Similar to the displacement gradient tensor $u_{i,j}$, the Cauchy stress can also be designated as the sum of the symmetric part σ_{ij} and the antisymmetric part τ_{ij},

$$t_{ij} = \sigma_{ij} + \tau_{ij}, \tag{20}$$

$$\sigma_{ij} = \frac{1}{2}\left(t_{ij} + t_{ji}\right), \tag{21}$$

$$\tau_{ij} = \frac{1}{2}\left(t_{ij} - t_{ji}\right). \tag{22}$$

Assuming that there is no volume force and volume moment, the equilibrium equations for the force and moment are

$$t_{ji,j} = 0, \tag{23}$$

$$m_{pi,p} = e_{ist}\tau_{st}. \tag{24}$$

Multiplying Eq. (24) by e_{ijk}, the equilibrium of moments becomes:

$$e_{ijk}m_{pi,p} = t_{kj} - t_{jk}. \tag{25}$$

Then, combining with Eq. (22), the equilibrium equation of moments becomes:

$$\frac{1}{2}e_{ijk}m_{pi,p} = -\tau_{jk}. \tag{26}$$

By substituting Eq. (26) and Eq. (20) into the equilibrium equation of the force in Eq. (23), a new equilibrium equation which covers the equilibrium of both the force and the moment is obtained as

$$\sigma_{ji,j} + \frac{1}{2}e_{ijk}m_{pk,pj} = 0. \tag{27}$$

For the strain gradient theory, the principle of virtual work is

$$\int_{\tilde{V}} \left(\sigma_{ij}\delta\varepsilon_{ij} + m_{ji}\delta\chi_{ij}\right)dV = \int_{\tilde{S}} \left(\bar{T}_i\delta u_i + \bar{M}_i\delta\omega_i\right)dS, \tag{28}$$

where the surface force and surface moment are

$$\bar{T}_i = \tau_{ji}n_j, \quad \bar{M}_i = m_{ji}n_j, \tag{29}$$

respectively, and n_j is the unit normal vector.

In this research, the overall stress and strain are represented by the hydrostatic part $\left(\sigma_m, \varepsilon_m\right)$ and the deviator part $\left(\boldsymbol{\Sigma}, \boldsymbol{\Omega}\right)$, where the generalized strain $\boldsymbol{\Omega} = \left(\mathbf{e}, l\boldsymbol{\chi}\right)$ and the generalized stress $\boldsymbol{\Sigma} = \left(\mathbf{S}, l^{-1}\mathbf{m}^T\right)$ are introduced, and l is the material intrinsic length. Similar to the Von Mises definition, the effective rotational gradient $\tilde{\chi}$ and the effective couple stress $\tilde{m}$ are defined as follows respectively:

$$\tilde{\chi} = \sqrt{\frac{2}{3}\chi_{ij}\chi_{ij}}, \quad \tilde{m} = \sqrt{\frac{3}{2}m_{ij}m_{ij}}. \tag{30}$$

Furthermore, the effective generalized strain $\tilde{\Omega}$ and the effective generalized stress $\tilde{\Sigma}$ are determined as:

$$\tilde{\Omega} = \sqrt{\frac{2}{3}\boldsymbol{\Omega}:\boldsymbol{\Omega}} = \sqrt{\tilde{e}^2 + l^2\tilde{\chi}^2}, \quad \tilde{\Sigma} = \sqrt{\frac{3}{2}\boldsymbol{\Sigma}:\boldsymbol{\Sigma}} = \sqrt{\tilde{S}^2 + l^{-2}\tilde{m}^2}, \tag{31}$$

where the effective deviator strain is $\tilde{e} = \sqrt{\frac{2}{3} e_{ij} e_{ij}}$ and the effective deviator stress is $\tilde{S} = \sqrt{\frac{3}{2} S_{ij} S_{ij}}$. With consideration of the rotational gradient, the work rate $\dot{w}$ per unit volume contains the contribution of both the strain and the rotational gradient, as giving

$$\dot{w}\left(\dot{\tilde{\Omega}}, \dot{\varepsilon}_m\right) = \sigma_{ij} \dot{\varepsilon}_{ij} + m_{ji} \dot{\chi}_{ij} = S_{ij} \dot{e}_{ij} + m_{ji} \dot{\chi}_{ij} + \sigma_m \dot{\varepsilon}_m \tag{32}$$

where $\dot{x}$ stands for the rate of x .

Similar to the strain which is the sum of elastic and plastic strain, the rotational gradient χ_{ij} is decomposed into the elastic rotational gradient χ_{ij}^e and the plastic one χ_{ij}^p . For the elastoplastic deformation, the work rate is then partitioned into an elastic energy density and a plastic energy density. The elastic generalized strain $\left(\mathbf{e}^e, l\boldsymbol{\chi}^e\right)$ is assumed to be related to the generalized stress $\left(\mathbf{S}, l^{-1}\mathbf{m}\right)$ via the elastic strain energy w^e, giving

$$e_{ji} = \frac{\partial w^e}{\partial s_{ij}}, \qquad l^{-1} m_{ji} = \frac{\partial w^e}{l \partial \chi_{ij}}, \tag{33}$$

where

$$w^e = \frac{E}{2(1+\nu)} \left[\frac{\nu}{1-2\nu} \varepsilon_m^2 + e_{ij}^e e_{ij}^e + l_{el}^2 \chi_{ij}^e \chi_{ij}^e \right]. \tag{34}$$

The elastic length scale l_{el} has no physical significance and is introduced in order to partition the gradient tensor into its elastic part and the plastic part (Fleck and Hutchinson, 1993). Substituting Eq. (33) into Eq. (34), the constitutive relationship is then determined as:

$$S_{ij} = D_{ijkl}^e e_{kl}^e, \quad l^{-1} m_{ji} = M_{ijkl}^e l \chi_{kl}^e. \tag{35}$$

where

$$D_{ijkl}^e = \frac{E}{(1+\nu)} \delta_{ik} \delta_{jl}, \qquad M_{ijkl}^e = \frac{E}{(1+\nu)} \left(\frac{l_{el}}{l} \right)^2 \delta_{ik} \delta_{jl}. \tag{36}$$

A prescription is now given for the viscoplastic part in the presence of the rotational

gradient and the couple stress. With consideration of the couple stress, the yield function generalizes to

$$\Phi\left(\boldsymbol{\Sigma}, Y\right)=\tilde{\Sigma}\left(\mathbf{S}, l^{-1}\mathbf{m}^{T}\right)-Y=0, \tag{37}$$

where Y is the current flow stress. The difference between Eq. 30 and classical yield function is that the effective stress σ_e is replaced by the generalized effective stress $\tilde{\Sigma}$ in the couple stress version of theory.

Based on the elasto-viscoplastic model, the constitutive relationship for the viscoplastic part is concluded from Eqs. (5) to (9), as giving,

$$\begin{cases} \tilde{S}=\sigma_{flow}+\sigma_{back} \\ \dot{\tilde{e}}^{p}=\dot{\varepsilon}_0 \exp\left(-\dfrac{\Delta H}{k_B \vartheta}\right)\left[\sinh\left(\dfrac{\bar{\sigma}V}{2k_B\vartheta}\right)\right]^{1/m} \\ \bar{\sigma}=\sigma_{flow}-s \\ \sigma_{back}=C_R\dfrac{\sqrt{n}}{3}\left[L^{-1}\left(\dfrac{1+\tilde{e}^{p}}{\sqrt{n}}\right)-\left(1+\tilde{e}^{p}\right)^{3/2}L^{-1}\left(\dfrac{1}{\left(1+\tilde{e}^{p}\right)^{1/2}\sqrt{n}}\right)\right] \end{cases}, \tag{38}$$

and the current flow stress Y is obtained from this equation.

Similar to the classical continuum theory, the plastic flow rule for the associated plasticity may be described as

$$\dot{e}_{ij}^{p}=\dot{\lambda}\frac{\partial\Phi}{\partial S_{ij}}, \quad \dot{\chi}_{ij}^{p}=\dot{\lambda}\frac{\partial\Phi}{\partial m_{ji}}, \tag{39}$$

where $\dot{\lambda}$ is the flow factor, $\dfrac{\partial\Phi}{\partial S_{ij}}$ and $\dfrac{\partial\Phi}{\partial m_{ji}}$ are the directions of plastic flow. According to the effective stress definition Eq. (31) and the yield function Eq. (37), the flow directions are derived as:

$$\frac{\partial\Phi}{\partial S_{ij}}=\frac{3S_{ij}}{2\tilde{\Sigma}}, \quad \frac{\partial\Phi}{\partial m_{ij}}=\frac{3m_{ij}}{2l^{2}\tilde{\Sigma}}. \tag{40}$$

According to yield function Eq. (37), the plastic consistency condition is:

$$\dot{\Phi} = \frac{\partial \Phi}{\partial S_{ij}} \dot{S}_{ij} + \frac{\partial \Phi}{\partial m_{ij}} \dot{m}_{ij} + \frac{\partial \Phi}{\partial Y} \dot{Y} = 0. \tag{41}$$

On the substitution of Eq. (35) and Eq. (39) into Eq. (41), the following is given:

$$\dot{\tilde{\Omega}}^p = \frac{1}{A} \left(\frac{\partial \Phi}{\partial S_{ij}} D^e_{ijkl} \dot{\varepsilon}_{kl} + \frac{\partial \Phi}{\partial m_{ij}} M^e_{ijkl} l^2 \dot{\chi}_{kl} \right), \tag{42}$$

where the effective plastic generalized stain is defined as

$$\dot{\tilde{\Omega}}^p = \sqrt{\left(\frac{2}{3} \dot{e}^p_{ij} \dot{e}^p_{ij} \right)^2 + l^2 \left(\frac{2}{3} \dot{\chi}^p_{ij} \dot{\chi}^p_{ij} \right)^2}, \tag{43}$$

the parameter A is determined by

$$A = \frac{\partial \Phi}{\partial S_{ij}} D^e_{ijkl} \frac{\partial \Phi}{\partial S_{kl}} + \frac{\partial \Phi}{\partial m_{ij}} M^e_{ijkl} l^2 \frac{\partial \Phi}{\partial m_{kl}} + H, \tag{44}$$

and H is the tangent modulus and is obtained by $H = \dfrac{\partial Y}{\partial \tilde{\Omega}^p}$.

Taking Eq. (36) and Eq. (40) into Eq. (44), it is obtained that

$$A = H + 3G \left(\frac{3}{2} \frac{S_{ij}}{\tilde{\Sigma}} \frac{S_{ij}}{\tilde{\Sigma}} + \frac{3}{2} \left(\frac{l_{el}}{l} \right)^2 \frac{m_{ij}}{l\tilde{\Sigma}} \frac{m_{ij}}{l\tilde{\Sigma}} \right), \tag{45}$$

where the shear modulus G is determined as $G = \dfrac{E}{2(1+\nu)}$.

According to Eq. (35), the deviator stress rate $\dot{S}_{ij}$ and the couple stress rate $\dot{m}_{ij}$ are

$$\dot{S}_{ij} = D^e_{ijkl} \left(e_{kl} - e^p_{kl} \right), \quad l^{-1} m_{ji} = M^e_{ijkl} l \left(\chi_{kl} - \chi^p_{kl} \right). \tag{46}$$

On the substitution of Eq. (39) and the effective plastic strain Eq. (43) into the above equation, the constitutive model with presence of size effect is obtained,

$$\dot{S}_{ij} = \left(D^e_{ijkl} - D^p_{ijkl} \right) \dot{\varepsilon}_{kl} - D^c_{ijkl} l \dot{\chi}_{kl}, \tag{47}$$

$$l^{-1} \dot{m}_{ij} = \left(M^e_{ijkl} - M^p_{ijkl} \right) l \dot{\chi}_{kl} - M^c_{ijkl} \dot{\varepsilon}_{kl}, \tag{48}$$

where:

$$D_{ijkl}^{p}=\frac{1}{A}D_{ijst}^{e}\frac{\partial\Phi}{\partial S_{st}}\frac{\partial\Phi}{\partial S_{mn}}D_{mnkl}^{e}, \tag{49}$$

$$D_{ijkl}^{c}=\frac{1}{A}D_{ijst}^{e}\frac{\partial\Phi}{\partial S_{st}}\frac{\partial\Phi}{\partial m_{mn}}M_{mnkl}^{e}l, \tag{50}$$

$$M_{ijkl}^{p}=\frac{1}{A}M_{ijst}^{e}l\frac{\partial\Phi}{\partial m_{st}}\frac{\partial\Phi}{\partial m_{mn}}M_{mnkl}^{e}l, \tag{51}$$

$$M_{ijkl}^{c}=\frac{1}{A}M_{ijst}^{e}l\frac{\partial\Phi}{\partial m_{st}}\frac{\partial\Phi}{\partial S_{mn}}D_{mnkl}^{e}. \tag{52}$$

Substituting Eq. (36) and Eq. (40) into Eqs. (49) to (52) and presenting the strain gradient elasto-viscoplastic model in matrix, it is obtained that

$$\dot{\mathbf{S}}=\left(\mathbf{D}^{e}-\mathbf{D}^{p}\right):\dot{\boldsymbol{\varepsilon}}-\mathbf{D}^{c}:l\dot{\boldsymbol{\chi}}, \tag{53}$$

$$l^{-1}\dot{\mathbf{m}}=\left(\mathbf{M}^{e}-\mathbf{M}^{p}\right):l\dot{\boldsymbol{\chi}}-\mathbf{M}^{c}:\dot{\boldsymbol{\varepsilon}}, \tag{54}$$

Where:

$$D_{ijkl}^{p}=\frac{9G^{2}S_{ij}S_{kl}}{\tilde{\Sigma}^{2}\left(H+3G_{m}\right)}, \tag{55}$$

$$D_{ijkl}^{c}=\left(\frac{l_{e}}{l}\right)^{2}\frac{9G^{2}S_{ij}m_{kl}}{\tilde{\Sigma}^{2}l\left(H+3G_{m}\right)}, \tag{56}$$

$$M_{ijkl}^{p}=\left(\frac{l_{e}}{l}\right)^{4}\frac{9G^{2}m_{ij}m_{kl}}{\tilde{\Sigma}^{2}l^{2}\left(H+3G_{m}\right)}, \tag{57}$$

$$M_{ijkl}^{c}=\left(\frac{l_{e}}{l}\right)^{2}\frac{9G^{2}m_{ij}S_{kl}}{\tilde{\Sigma}^{2}l\left(H+3G_{m}\right)}, \tag{58}$$

and

$$G_{m}=G\left[\frac{3S_{ij}S_{ij}}{2\tilde{\Sigma}^{2}}+\left(\frac{l_{e}}{l}\right)^{2}\frac{3m_{ij}m_{ij}}{2l^{2}\tilde{\Sigma}^{2}}\right]. \tag{59}$$

If $l_{e}=l$, G_{m} is then converged into the shear modulus G. In addition, the volume component is also assumed to remain in the linear elastic relationship as:

$$\sigma_m = \frac{3E}{1-2\nu}\varepsilon_m. \tag{60}$$

It should be pointed out that the intrinsic material lengths are defined to meet the demand for dimensional consistency in the present research so that the proposed strain gradient elasto-viscoplastic model is a phenomenon model to represent the size effect of amorphous polymers in micro-scale. When the feature scale is in the order of the intrinsic material length, the impact of rotational gradient becomes so significant that should not be ignored. When the feature scale is far greater than the intrinsic material length, the developed strain gradient elasto-viscoplastic model is converged to the elasto-viscoplastic model.

4. Experiments

4.1 Sample preparations

Before micro-bending experiments, PMMA plates with different thicknesses were prepared in lab for micro-bending experiments. First of all, commercial PMMA granules were dried and molded into PMMA plates, at the temperature of 175 ^{o}C and the compression pressure of 20 MPa for 30 mins. Then, PMMA plates were cooled to room temperature under the pressure of 5 MPa before demolding. After that, annealing process was performed on the processed PMMA plates in a vacuum furnace which maintained at the temperature of 115 ^{o}C for 2 h and then gradually cooled down to room temperature in another 10 h, in order to eliminate the residual stress and minimize the original difference between PMMA plates with different thicknesses. After that, PMMA plates with six different thicknesses were prepared and both the average thickness and the standard deviation of the plates are displayed in Table 2.

Table 2

Average and standard deviation of thicknesses of PMMA plates

Sample No.	1	2	3	4	5	6
Average thickness (mm)	0.268	0.376	0.473	0.665	1.014	1.979
Standard deviation (mm)	0.017	0.018	0.011	0.016	0.032	0.024

In order to understand the original differences between these PMMA plates, both the surface and the interior mechanical behaviors of PMMA plates were measured by the nanoindenter (Hysitron TriboIndenter, USA). All nanoindentations were made by a diamond Berkovich tip under the room temperature with the maximum load of 5 mN, loading time of 1 s, holding time of 1 s and unloading time of 1 s. Three repeated tests were performed for each set of measurements and the resulting data were averaged. Firstly, the reduced modulus and the hardness at the surface of both as-processed and annealed PMMA plates were measured, as shown in Fig. 4. The standard errors of both the reduced modulus and the hardness of the annealed PMMA plates get smaller than that of the as-processed plates. Moreover, both the reduced modulus and the hardness fluctuate less with the thickness when the PMMA plates are annealed. It illustrates that the appropriate annealing process efficiently reduces the original differences among PMMA plates.

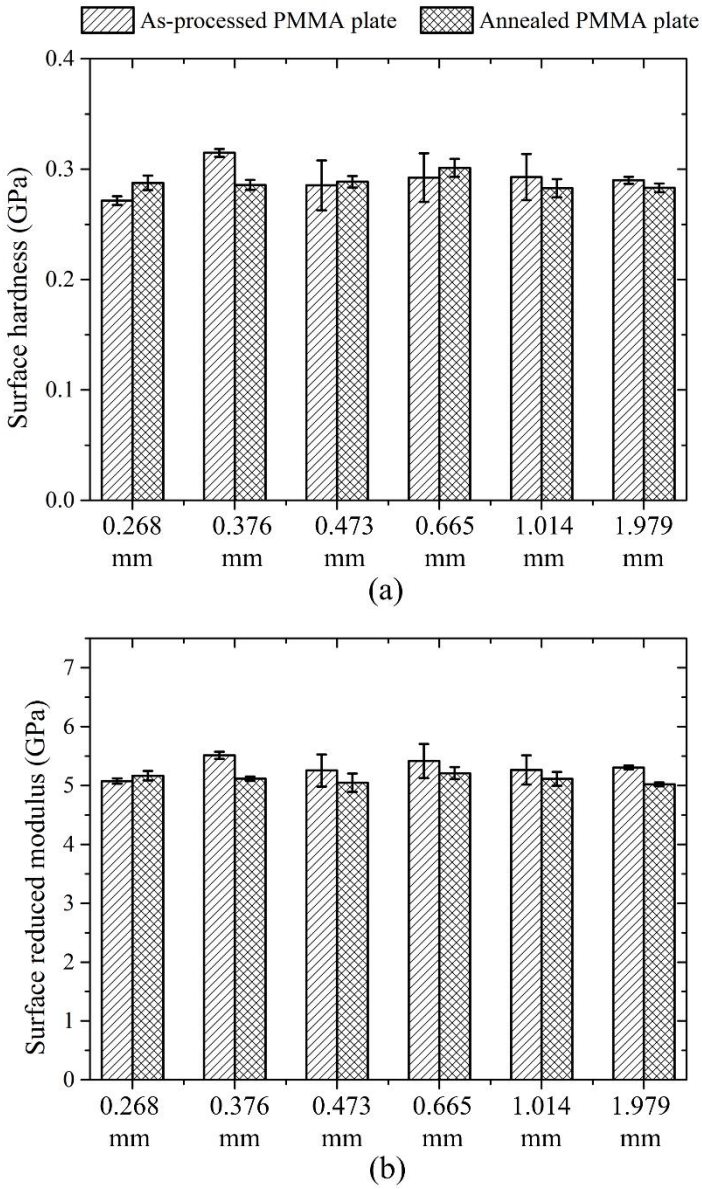

Fig. 4. Surface reduced modulus (a) and surface hardness (b) of as-processed and annealed PMMA plates.

In addition, internal mechanical behaviors of annealed PMMA materials were testes via nanoindentations on the thickness sections. The tested samples included six plate samples prepared for micro-bending experiments and compression samples with thickness of 9 mm used for the study of elasto-viscoplastic behaviors of polymers in Section 3.1. For each sample, six indentations were made with evenly space from the top surface to the bottom surface along the thickness direction. However, because the PMMA samples were mosaiced

for measurements on sections, the results of the first and sixth indentations cannot represent the true behaviors of PMMA samples and only information of the middle four indentations was applied for discussions. Fig. 5 shows the internal reduced modulus and internal hardness against the normalized position at the thickness section of annealed PMMA samples. For each sample, both the internal reduced modulus and the internal hardness fluctuate little over the normalized position at its thickness section. Particularly, the differences between its internal reduced moduli through the thickness direction are below 6.3% and those between its internal hardnesses through the thickness direction are less than 4.3%. It can be concluded that the mechanical behaviors in the PMMA samples get uniform after annealing process.

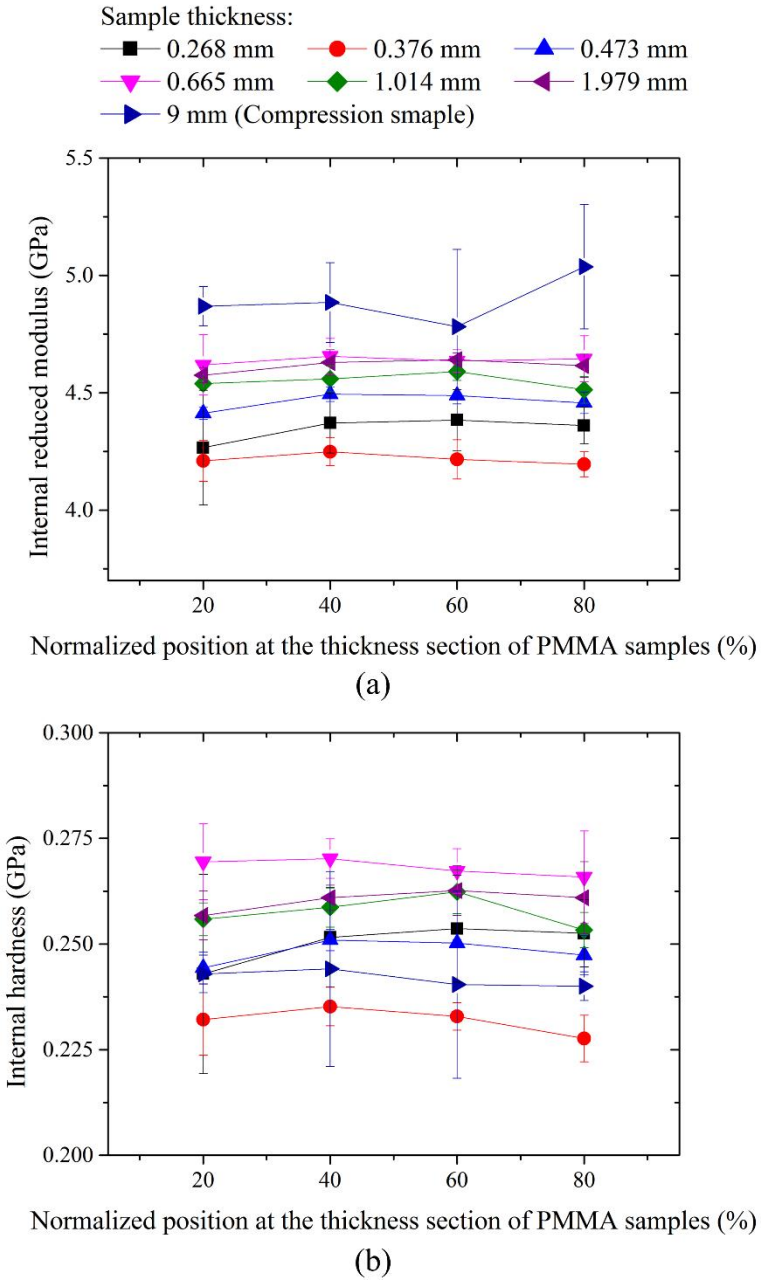

Fig. 5. (a) Internal reduced modulus against the normalized position and (b) internal hardness against the normalized position of annealed PMMA samples.

Furthermore, the internal reduced moduli and internal hardnesses are averaged for each annealed sample and the results are shown in Fig. 6. For both the internal reduced moduli and internal hardnesses, the average values fluctuate in a narrow range over the thicknesses: the averages of internal reduced moduli vary from 4.17 to 4.89 GPa and those data of internal

hardnesses change from 0.23 to 0.27 GPa. Additionally, the average behaviors of the annealed PMMA samples fluctuate randomly with the thicknesses and do not show any regular variation. In this case, the annealed PMMA plates can be used for the experimental study of the size effect behaviors of amorphous polymers and the possibility of size effect of amorphous polymers caused by the original differences between samples is efficiently eliminated by the annealing process.

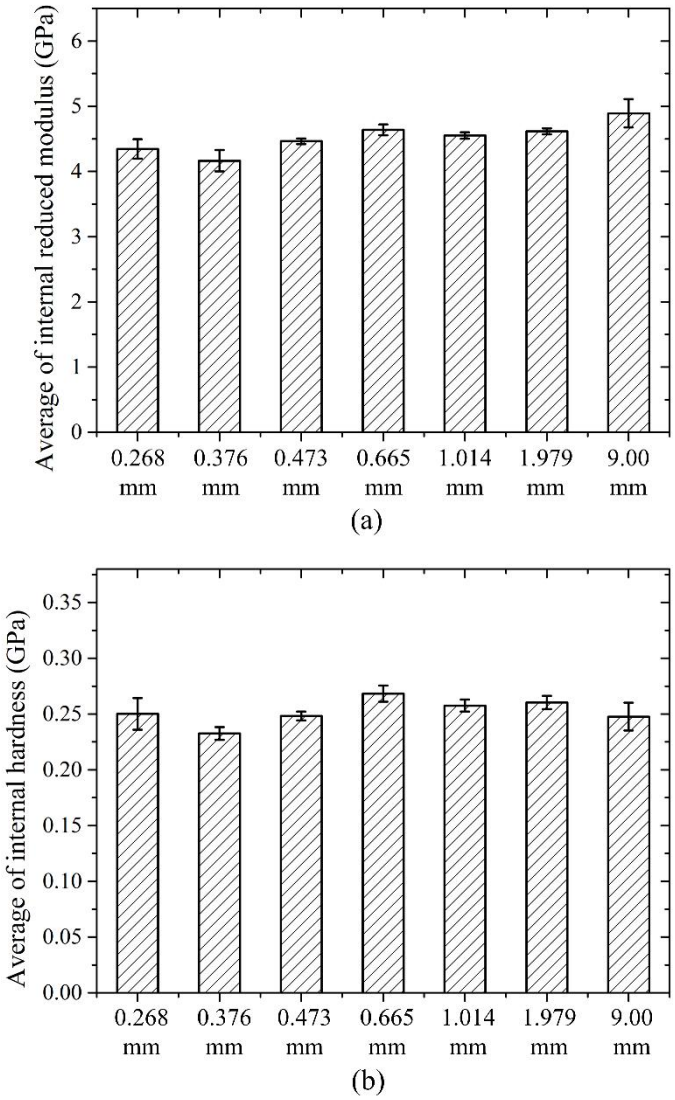

Fig. 6. (a) Average of internal reduced modulus and (b) average of internal hardness of annealed PMMA samples.

Lastly, the annealed PMMA plates were cut into micro-bending beams with various

thicknesses and each section of the beams was further polished to minimize the cracks. The ratio of the width to the thickness was larger than 30 to realize the plane-strain deformation of the beams.

4.2 Four-point micro-bending experiments

A four-point micro-bending setup was established as shown in Fig. 7. This setup includes a micro-bending tool, a material testing machine and a digital camera, as can be seen in Fig. 7 (a). A MTS testing machine equipped with a force sensor with the maximum load of 1 kN was used to record the bending force, and a digital camera (MV-3000 UC, three megapixels' resolution) with a variable magnification (from × 0.7 to × 4.5) was used to take photos from the beam continuously during the bending process. Additionally, Fig. 7 (b) shows the four-point micro-bending tool with details. In the micro-bending tool, there were a pair of upper fixtures supporting two round bars and a pair of lower fixtures supporting another two round bars. PMMA beams were supported and bended by the upper round bars and the lower round bars which acted as the four points during micro-bending tests. In addition, four pairs of linear bearing were used as guide columns.

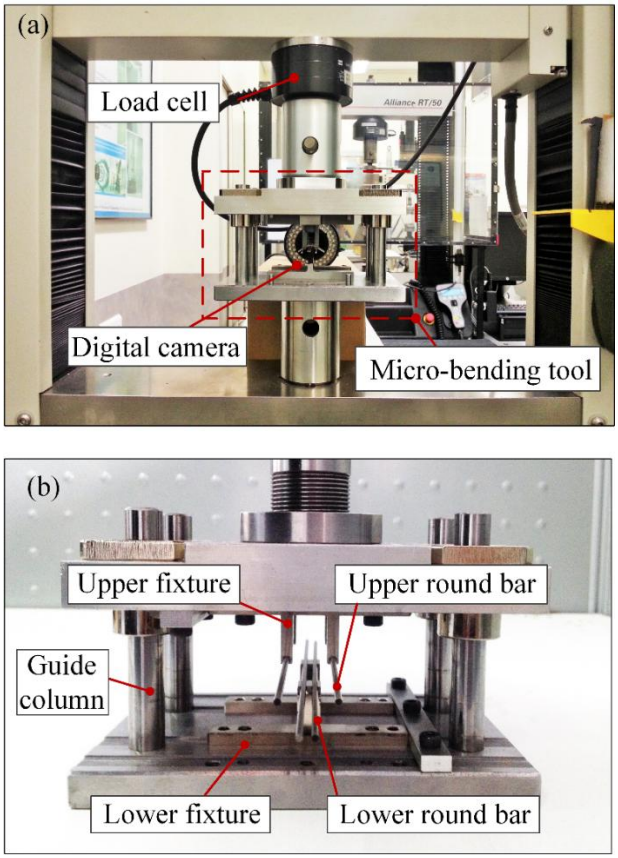

Fig. 7. (a) Micro-bending platform and (b) four-point micro-bending tool for four-point micro-bending experiments.

Among micro-bending process of PMMA plates, the digital camera took photos of the beam every three seconds. Then, the curvature of the middle of the beam could be conveniently obtained by image processing of the photos of bended beams because the middle of the beam had the same curvature during four-point micro-bending. After the curvature was known, more information on the strain was available for the bending solution. From this point of view, four-point micro-bending is more convenient for the size effect study of materials, compared with three-point micro-bending (Stölken and Evans, 1998) as well as the cantilever micro-bending (Li et al., 2011). Additionally, the changed load and the changed curvature over time were recorded. For each condition, the micro-bending experiments were

repeated at least three times to achieve the average value and the standard error of the experimental data.

5. Results and discussions

5.1 Pure bending based on strain gradient theory

In the present research, the thickness of the polymeric sample is defined to be much smaller than its length and width. Therefore, it is acceptable to assume that four-point micro-bending of polymeric film is plane-strain pure bending problem. Fig. 8 shows the schematic of pure bending in plane-strain state. The mid-plane of the thin plane-strain beam (an infinitely wide plate) is set as the x–y plane in a Cartesian coordinate system and z-axis is set along the width direction. In plane-strain state, the beam deformation is independent of the width coordinate z and no shear strain happens in the pure bending beam. For simplification, the body force in the beam is also ignored and the neutral surface, which is neither compressed nor extended, is assumed to be located at the mid-plane of the beam during the bending process.

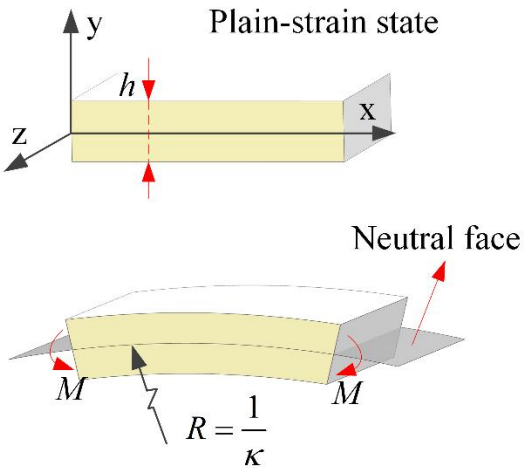

Fig. 8. Schematic diagram of the pure bending in plane-strain state.

The pure bending problem without considering the size effect was analyzed firstly, on the

basis of the elasto-viscoplastic model of amorphous polymers in macro-scale and the material parameters of PMMA materials in Table 1 were used here for analysis. Fig. 9 (a) shows the surface strain of the beam with the y coordination of $h/2$, $\kappa h/2$, against bending time. With the increase of bending time, the total surface strain increases linearly. Particularly, when the total strain is smaller than 0.02, the elastic strain increases linearly and the plastic part maintains at nearly zero. While the total strain is larger than 0.02, the plastic strain in the surface layer of the beam increases beyond zero and then yielding gradually extends from the surface layer to the area near the neutral layer of the beam. Additionally, Fig. 9 (b) shows the normalized bending moment, $M_{nor} = 4M/bh^2$, against the surface strain. When the surface strain is smaller than 0.02, the bending moments predicted by the linear elastic model overlap those by elasto-viscoplastic model. Hence, for PMMA materials, pure bending without consideration of the size effect is elastic as the surface strain is less than 0.02 and exhibits elastoplastic behaviors when the surface strain is larger than 0.02. In this way, the following experiments and analysis of micro-bending with presence of size effect are correspondingly implemented from the aspect of elastic micro-bending and elastoplastic micro-bending for the size effect study of amorphous polymers in micro-scale.

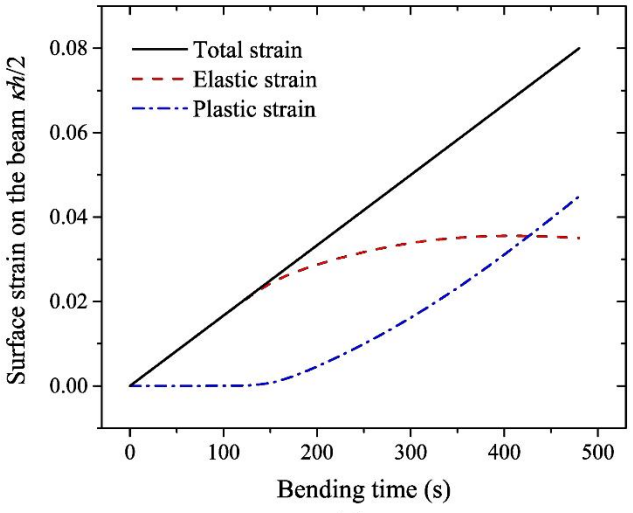

(a)

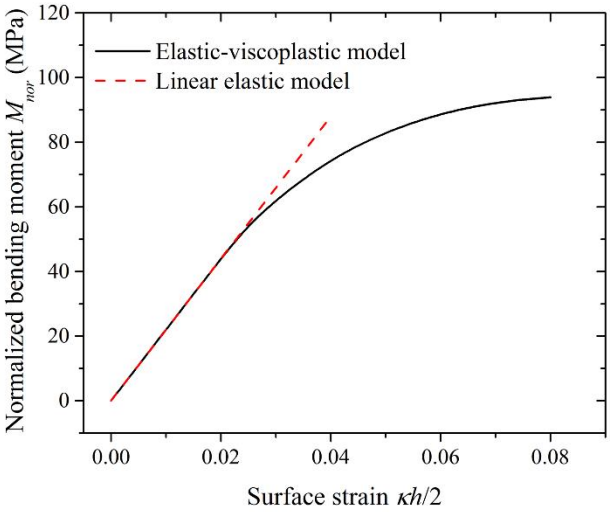

(b)

Fig. 9. (a) Surface strain against bending time and (b) the normalized bending moment against surface strain obtained from pure bending solution for the PMMA without consideration of the size effect.

On the one hand, for elastic micro-bending problem with considering size effect, the non-zero components of the strain and stress can be represented as:

$$\varepsilon_{xx} = \kappa y, \quad \varepsilon_{yy} = -\frac{\nu}{1-\nu}\kappa y, \tag{61}$$

and

$$\sigma_{xx} = \frac{E}{1-\nu^2}\kappa y, \quad \sigma_{zz} = \frac{\nu E}{1-\nu^2}\kappa y. \tag{62}$$

According to the definition of the rotational gradient in Eq. (19), the non-zero component of rotational gradient χ_{ij} for this case is χ_{xz} as giving

$$\chi_{xz} = -\kappa, \tag{63}$$

Based on the constitutive relationship Eq. (36), the non-zero component of couple stress m_{ij} is

$$m_{zx} = -\frac{E}{1+\nu} l_{el} \kappa. \tag{64}$$

Considering the impact of the rotational gradient, the moment M of the beam is produced by stress σ_{xx} and the couple stress m_{xz} in the following:

$$M = 2b\left(\int_0^{h/2} \sigma_{xx} y dy - \int_0^{h/2} m_{xz} dy \right), \tag{65}$$

where b is the width of the beam and h is its thickness.

Substituting the stress in Eq. (62) and the couple stress in Eq. (64) into Eq. (65), the moment for elastic micro-bending is obtained as:

$$M = \frac{h^3 b}{12\left(1-\nu^2\right)} \left[1 + 12\left(1-\nu\right)\left(\frac{l_{el}}{h} \right)^2 \right] E\kappa. \tag{66}$$

Making $l_{el} = 0$, the moment M is reduced to the classical expression of the elastic micro-bending in the following:

$$M = \frac{E}{\left(1-\nu^2\right)} I\kappa, \tag{67}$$

where the classical moment of inertia is $I = \frac{bh^3}{12}$.

On the other hand, for elastoplastic micro-bending problem with size effect, the solution procedure is more complicated because the normal strain in y-direction ε_{yy} becomes unknown. Here, an iteration approach was programmed with the help of MATLAB to solve

the elastoplastic micro-bending problem with size effect and the flow chart of the solution is presented in Fig. 10. In this iteration program, elastoplastic micro-bending problem was solved layer by layer in the beam because different layers of the beam have different strain rates. Then, the bending moment of the whole beam was determined using the method of the trapezoidal integral as

$$M = 2b\sum_{i=0}^{n}\left(\frac{y_{i+1}+y_i}{2}\sigma_{xx}\Big|_{h=\frac{y_{i+1}+y_i}{2}} - m_{xz}\right)\left(y_{i+1}-y_i\right), \tag{68}$$

where the beam was divided into $2n$ layers along the direction of the thickness and the y coordination was $y_i = \frac{i}{2n}h$. Actually, the larger n makes the bending moment closer to the exact solution. When n is larger than 4, the difference between the trapezoidal integral solution and the exact solution becomes less than 1%. Hence, each beam was divided into 8 layers for the following solutions in the present research.

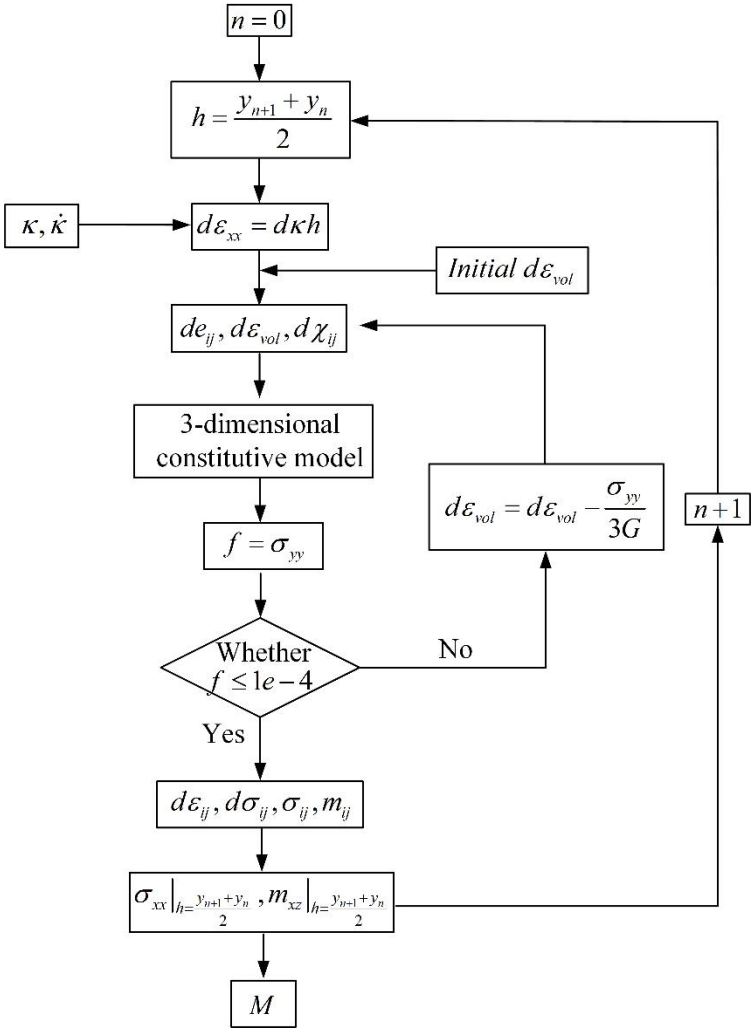

Fig. 10. Flow chart of the solution for the elastoplastic micro-bending.

For the solution in each layer of the beam, the curvature κ and the curvature rate $\dot{\kappa}$ obtained from micro-bending experiments are taken as input parameters. Then, the normal strain rate in x-direction $\dot{\varepsilon}_{xx}$ of this layer is determined by

$$\dot{\varepsilon}_{xx}=\dot{\kappa}y, \tag{69}$$

where y is the y-coordination of the layer. Based on these input parameters, each layer was solved with the combination of the proposed strain gradient elasto-viscoplastic model and the iterations. For the compressible material, the volume strain increment was set as the iteration variable and the equation $\sigma_{yy}=0$ was defined as the objective function. When the iteration converges, both the stress and couple stress of the layer became available. Lastly, according

to Eq. (68), the bending moment in this case was solved.

5.2 Size effect analyses

5.2.1 Size-dependent elasticity

According to the solution of the elastic bending without consideration of size effect in Eq. (67), the normalized bending moment M_{nor} is related to the surface strain $\kappa h/2$ linearly as

$$M_{nor}=\frac{4M}{bh^2}=\frac{2E}{3\left(1-\nu^2\right)}\left(\frac{\kappa h}{2}\right), \tag{70}$$

and the slope of elastic the normalized moment versus surface strain is defined as the elastic bending stiffness. According to Eq. (70), the classical elastic bending stiffness D_c without size effect is then determined as

$$D_c=\frac{2E}{3\left(1-\nu^2\right)}. \tag{71}$$

It is noted that the elastic bending stiffness only depends on the elastic modulus and the Poisson's ratio according to the classical theory. That is to say that the classical elastic bending stiffness should be a constant for a specified polymer even for different beam thicknesses. Fig. 11 shows the normalized bending moment against surface strain of the elastic micro-bending experiment for PMMA plate with thickness of 0.473 mm. The results present that the normalized bending moment increases linearly with the surface strain of the PMMA beam. After linear fitting the experimental data, the elastic bending stiffness of this PMMA plate is determined as 3007 MPa.

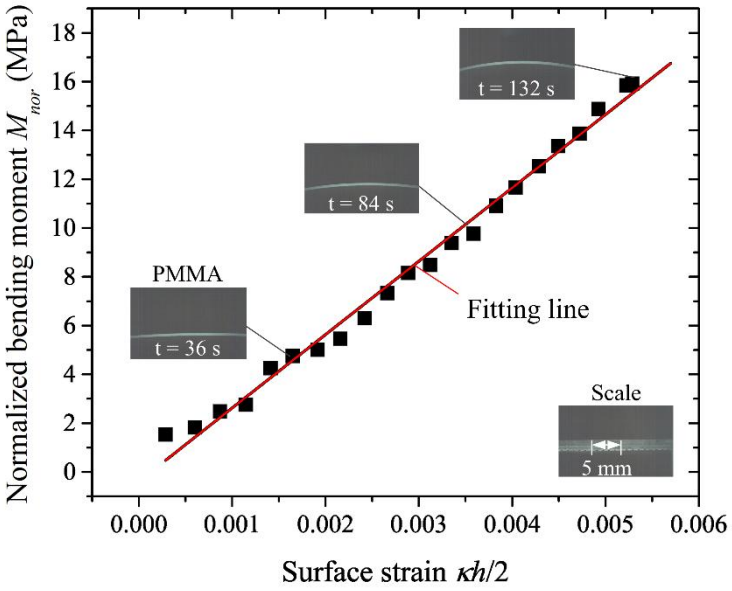

Fig. 11. The normalized bending moment against surface strain of elastic micro-bending on the PMMA plate with the thickness of 0.473 mm.

More elastic micro-bending experiments were implemented on the PMMA plates with different thicknesses and the corresponding results are displayed in Fig. 12. From these experimental data in Fig. 12 (a), the relationships between the normalized bending moment and the surface strain are close to linearity even for different PMMA plates. However, the slopes of the normalized bending moment versus surface strain are different from each other and exhibit an increase tendency with the decrease of the beam thickness from 1.979 to 0.268 mm. Referring to the works by Li et al. (2011), Stölken and Evans (1998) and Suzuki et al (2009), the nondimensional bending moment was further defined to eliminate the impact of the original differences between the PMMA plates on the micro-bending results. For elastic micro-bending, the nondimenional bending moment of each sample was defined as the normalized bending moment divided by its average of internal reduced modulus E_R, namely $M_{non} = M_{nor} / E_R$. Fig. 12 (b) presents the relationship between the nondimensional bending moment and surface strain for different PMMA plates. The slopes of the nondimensional

bending moment versus surface strain also increase with the decrease of the thickness of the PMMA plate even when the original difference between samples is eliminated.

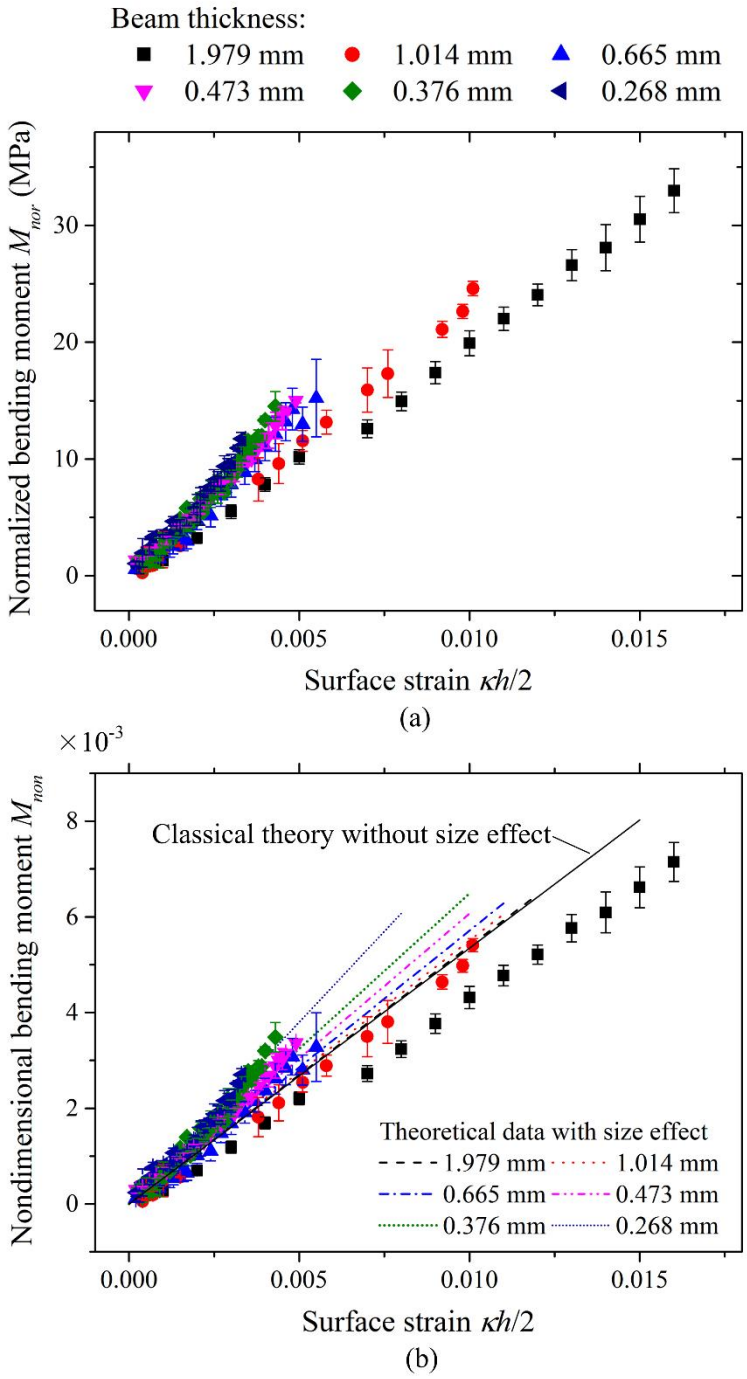

Fig. 12. (a) The normalized bending moment against surface strain and (b) the nondimensional bending moment against surface strain from elastic micro-bending experiments on PMMA plates with different thicknesses.

Moreover, the slope of the nondimensional bending moment versus surface strain was defined as the nondimensional bending stiffness. Correspondingly, Fig. 13 shows the elastic bending stiffness and the nondimensional bending stiffness against the beam thickness of PMMA. For PMMA plates with thickness of 1.979 and 1.014 mm, the elastic bending stiffnesses are 2164 and 2480 MPa, respectively. However, when the beam thickness decreases from 0.665 to 0.268 mm, the elastic bending stiffness increases from 2745 to 3160 MPa. After eliminating the original differences between the PMMA plates, the nondimensional bending stiffness also exhibits an increase of about 33% with the decrease of the PMMA thickness from 1.979 to 0.268 mm and shows a strong size-dependence which the classical theory cannot represent well.

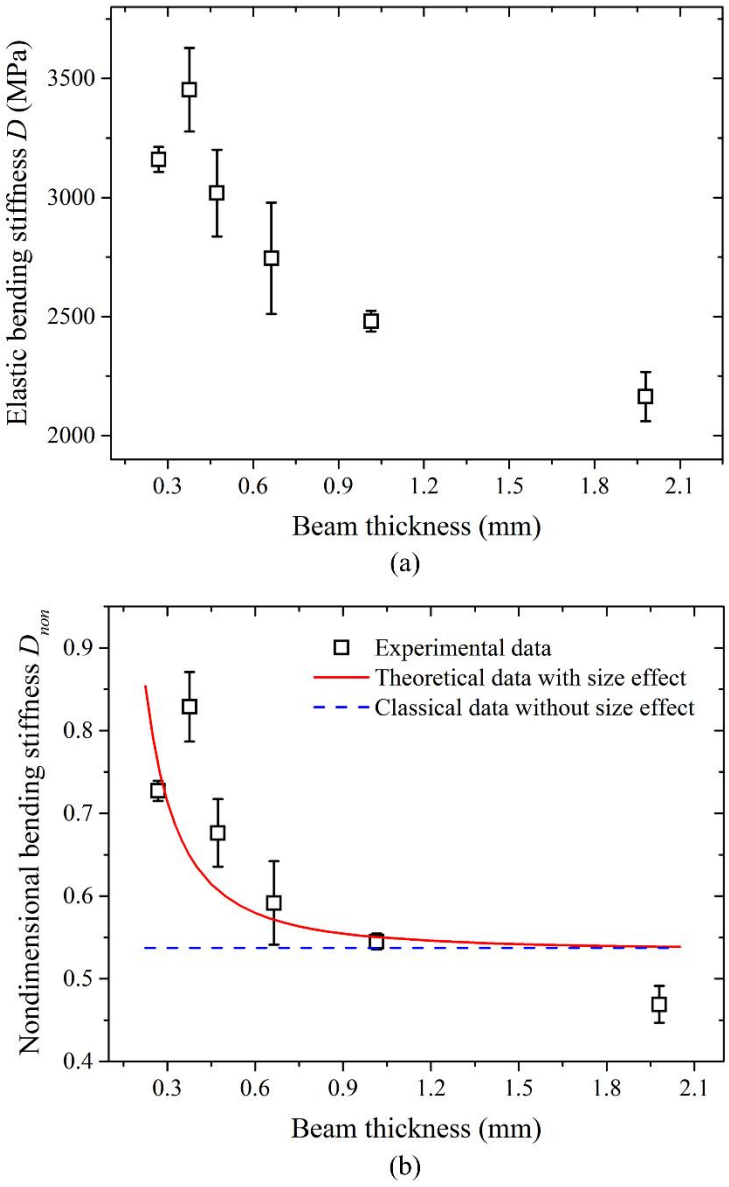

Fig. 13. (a) Elastic bending stiffness and (b) the nondimensional bending stiffness of PMMA plates.

In order to represent the size-dependent stiffness in the elastic micro bending, the impact of the rotational gradient is considered in the present work. According to the moment equation considering the rotational gradient in Eq. (66), the nondimensional bending stiffness is dependent on the beam thickness h and is determined as,

$$\frac{D}{E_R}=\frac{2E}{3\left(1-\nu^2\right)E_R}\left[1+12\left(1-\nu\right)\left(\frac{l_{el}}{h}\right)^2\right]. \tag{72}$$

It is noted that the elastic bending stiffness D in Eq. (72) can be converted into the classical elastic bending stiffness D_c in Eq. (71) when the beam thickness is far larger than the elastic intrinsic length l_{el}.

According to Eq. (72), the nondimensional bending stiffness obtained from experiments was fitted via weighted regression where the elastic intrinsic length and elastic modulus were set as the parameters to be fitted and the reciprocal of the standard error was set as the weighting factor. As a consequence, the elastic intrinsic length l_{el} was determined as 0.062 mm for PMMA materials. Additionally, elastic modulus was specified as 3441 MPa which was larger than the modulus calibrated via compression experiments. This was maybe due to the fact that the friction in guides might lead to a larger load and a harder stiffness during micro-bending experiments. Lastly, theoretical stiffness considering the size effect is plotted in both Fig. 12 (b) and Fig. 13 (b) with lines. After comparison analysis of those data, it is found that the proposed model with the size effect is converged to the classical model when the beam thickness is larger than 0.6 mm. In such condition, there is no big difference between the predicted data by the classical model and those by the proposed model considering the size effect. Moreover, the predicted results based on both models are tallied well with the experimental results. When the thickness of the PMMA plate is less than 0.6 mm, however, the nondimensional bending moments from micro-bending experiments are larger than the predicted moments based on the classical model. Although the elastic intrinsic length of PMMA is 0.062 mm, the effect of the rotational gradient becomes non-ignorable even when the thickness of PMMA is decreased into the order of 0.2 mm. Generally, compared with the classical model, the proposed model with consideration of the size effect

gives a much better prediction of the elastic behaviors of amorphous polymers in micro-scale.

5.2.2 Size dependent plasticity

Elastoplastic micro-bending experiments were then conducted and the corresponding results are shown in Fig. 14. From the experimental data in Fig. 14 (a), the normalized bending moment increases nonlinearly with the increase of the surface strain even for different PMMA plates. More importantly, the normalized bending moments of the thinner beams are larger than those of the thicker beams under the same surface strain. For elastoplastic micro-bending of each sample, the nondimensional bending moment is defined as the normalized bending moment divided by its average internal hardness H, namely $M_{non} = M_{nor} / H$. After eliminating the original difference of PMMA plates, as can be seen in Fig. 14 (b), the nondimensional bending moments also exhibit the mechanical strengthening for the thinner beams. According to the classical theory without size effect, the relationship between the nondimensional bending moment and surface strain in micro-bending should maintain the same even for different beam thicknesses. Hence, the classical theory cannot represent the observed the experimentally-observed strengthening plasticity of PMMA materials in micro-scale and the size effect of PMMA is thus demonstrated in micro-scale.

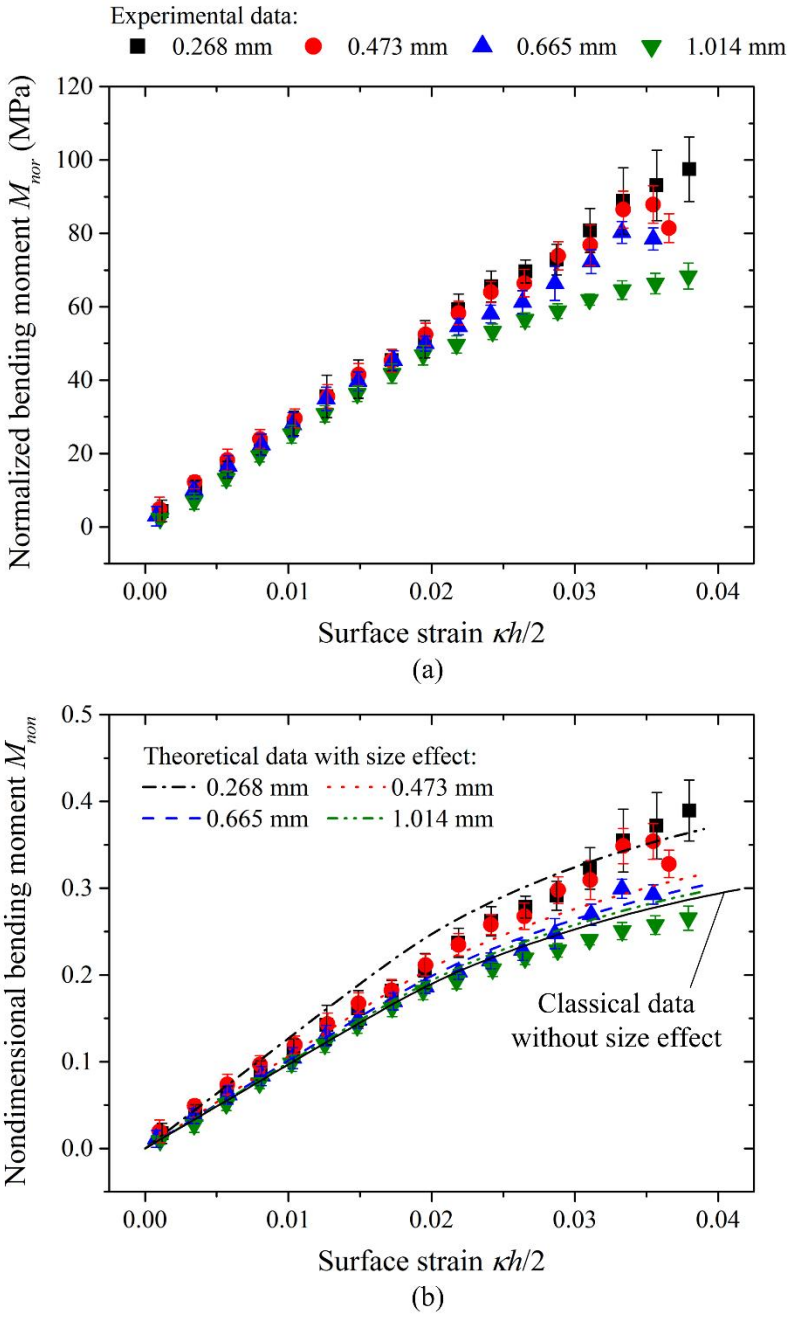

Fig. 14. (a) The normalized bending moment against surface strain and (b) the nondimensional bending moment against surface strain obtained from elastoplastic micro-bending experiments on different PMMA plates.

Furthermore, a difference between the nondimensional bending moments was defined as $\Delta M_{non} = M_{non} - M_{non-1.014mm}$ where $M_{non-1.014mm}$ is the nondimensional bending moment of the PMMA plates with the thickness of 1.014 mm. Fig. 14 shows the correspondingly

difference between the nondimensional bending moments against the beam thickness when the surface strain is 0.022, 0.027, 0.031 and 0.035, respectively. According to the classical theory, the difference for beams with different thicknesses should be zero. However, from the experimental results, the difference between the nondimensional bending moments increases beyond the classical value with the decrease of the beam thickness. This further demonstrates that the mechanical behavior of PMMA material in elastoplastic micro-bending is size-dependent.

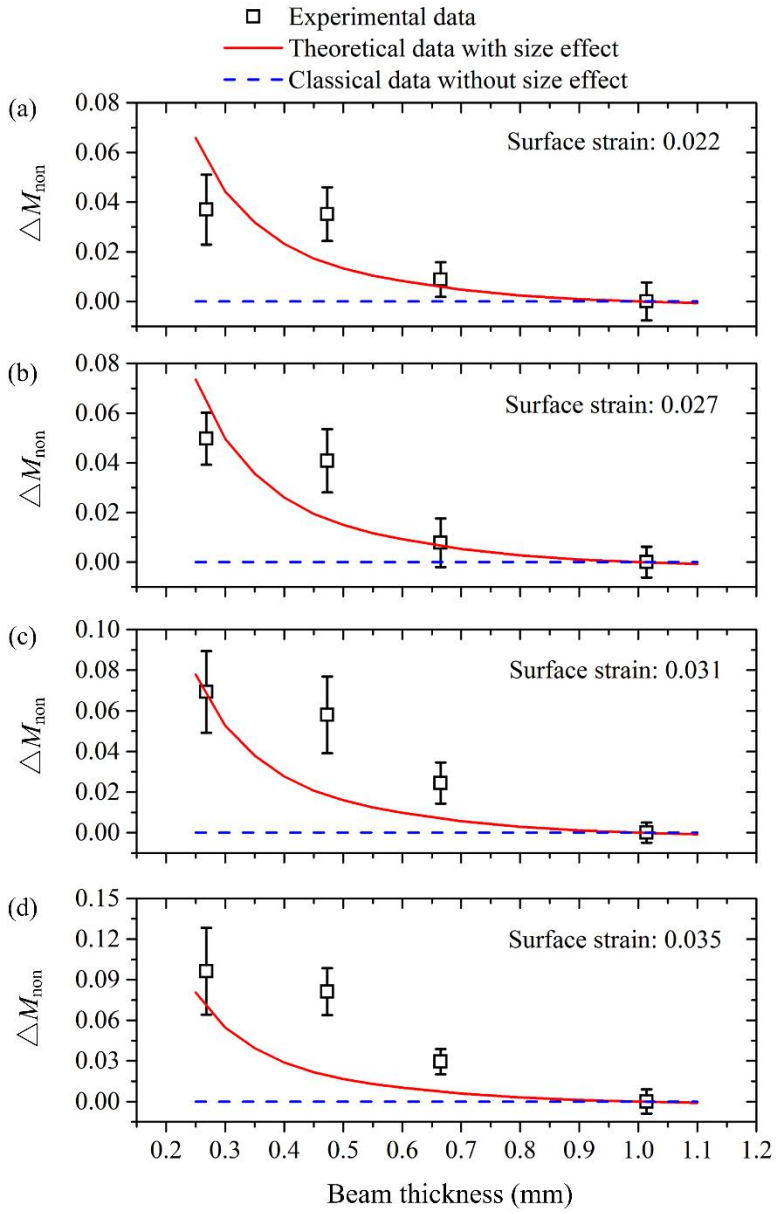

Fig. 15. Difference between the nondimensional bending moments against the beam thickness of PMMA at the surface strains of (a) 0.022, (b) 0.027, (c) 0.031 and (d) 0.035.

Based on the results of elastoplastic micro-bending, the plastic intrinsic material length was obtained via minimizing the quadratic sum of the difference between the experimental and the theoretical value of the proposed model with the size effect. It should be pointed out that the elastic modulus applied here was 3441 MPa which was obtained from elastic micro-bending experiments, for a better description of the elastoplastic micro-bending results. As a consequence, the plastic intrinsic length is determined as 0.034 mm for PMMA materials and the corresponding theoretical data are shown in both Fig. 14 (b) and Fig. 15 by lines. When the beam thickness is less than 0.6 mm, the difference between the experiments and the predicted ones based on the classical model gets increasingly large, while the proposed model with the size effect agrees better with the experimental results. This suggests that the size effect of PMMA can be represented well by the proposed strain gradient elasto-viscoplastic constitutive model.

Through micro-bending experiments, the elastic and plastic intrinsic lengths in the proposed strain gradient elasto-viscoplastic model were determined at 0.062 mm and 0.034 mm for PMMA materials, respectively. Previously, Lam et al. (2003) determined the elastic intrinsic length of epoxy materials at 0.024 mm according to micro-bending experiments and later Lam et al. (2010) specified the strain gradient length scale parameter associated with rotation gradients at 0.034 mm for epoxy based on creep bending experiments. In comparison, elastic and plastic intrinsic lengths of PMMA in the present study, are on the same order as those for epoxy materials obtained by Lam et al (2003) and Lam et al. (2010). Additionally, it

is also noted that the two intrinsic lengths are in the same order of the length. When the feature size is decreased to the order of tens of microns, both the elastic and plastic behaviors are strengthened and size-dependent. To control the dimensional accuracy and product quality, size effects on elastic and plastic behaviors are equally important and should be considered simultaneously.

6. Conclusions

Constitutive modeling under consideration of size effect for amorphous polymers in micro-scaled deformations was implemented in the present research, on the basis of the couple stress theory. The following concluding remarks are drawn:

1. In order to quantitatively predict and describe the size-dependent behaviors of amorphous polymers in micron scale, a strain gradient elasto-viscoplastic constitutive model was proposed via taking the impacts of the rotational gradient into considerations, on the basis of the couple stress theory. In this model, the size effect on both elastic and plastic behavior of amorphous polymers was represented simultaneously such that the size effect in micro-scale deformation can be modeled and analyzed more accurately.

2. Four-point micro-bending experiments were designed and carried out on PMMA plates for the purpose of experimental study on the size effect of amorphous polymers in micro deformations. After eliminating the original differences between the PMMA plates, the nondimensional bending stiffness increased to 1.33 times for elastic micro-bending and the nondimensional bending moment also exhibited an obvious mechanical strengthening for elastoplastic micro-bending when the beam thickness decreased from 1.979 to 0.268 mm. The experimental results of micron-bending on PMMA showed a strong size-dependence

which the classical theory cannot represent well.

3. Based on micro-bending results, the proposed strain gradient elasto-viscoplastic model was validated for PMMA materials. The elastic and plastic intrinsic lengths were determined as 0.062 and 0.034 mm, respectively. Two intrinsic lengths have the same order of length scale, which means the size effect on elastic and plastic deformation behaviors are equally important for amorphous polymers. Lastly, the strain gradient elasto-viscoplastic model was verified for the capability for a good representation of the size effect of amorphous polymers in micro deformation.

Acknowledgements

This study is supported by the National Natural Science Foundation of China (No 51235008, 51421092), and the program of Shanghai Subject Chief Scientist (No. 13XD1402200). The project is also supported by the General Research Fund of Hong Kong Government under the project of 515012 (B-Q33F).

Appendix

Nomenclature

w	Deformation energy density	t_{ij}	Cauchy stress
σ_{ij}	Symmetric stress tensor	τ_{ij}	Antisymmetric stress tensor
u_i	Displacement	ε_{ij}	Strain tensor
ω_{ij}	Curl tensor	θ_i	Rotation vector
$\boldsymbol{\Sigma}$	Generalized stress	$\boldsymbol{\Omega}$	Generalized strain
$\tilde{\Sigma}$	Effective generalized stress	$\tilde{\Omega}$	Effective generalized strain
$\overline{T}_i$	Surface force	$\overline{M}_i$	Surface moment

σ_m	Hydrostatic pressure	S_{ij}	Deviator stress
$\tilde{S}$	Effective deviator stress	m_{ij}	Couple stress
$\tilde{m}$	Effective couple stress	$\dot{\tilde{\varepsilon}}$	Effective strain rate
$\tilde{e}$	Effective deviator strain	ε_m	Volumetric strain
e_{ij}	Deviator strain	$\dot{e}_{ij}^{e}$	Elastic strain rate
e_{ij}^{e}	Elastic deviator strain	e_{ij}^{p}	Plastic strain
e_{ij}^{p}	Plastic strain rate	$\tilde{e}^{p}$	Effective plastic strain
$\dot{\tilde{e}}^{p}$	Effective plastic strain rate	$\tilde{\chi}$	Effective rotational gradient
χ_{ij}	Rotational gradient	χ_{ij}^{e}	Elastic rotational gradient
χ_{ij}^{p}	Plastic rotational gradient	E	Young's modulus
D_{ijkl}	Classical elastic stiffness	X_E	The variation of the Young's modulus with strain rate
E^{ref}	Reference Young's modulus	ν	Poisson's ratio
ϑ	Temperature	C_R	Rubber modulus
σ_{back}	Back stress in Langevin model	X_C	The variation of the rubber modulus with strain rate
C_R^{ref}	Reference rubber modulus	σ_{flow}	Flow stress in Eyring model
$n^{1/2}$	Factor limiting network strain in Langevin model	ΔH	Activation energy of Eyring model
$\dot{\varepsilon}_0$	A pre-exponential factor of Eyring model	V	Shear activation volume of Eyring model
k_B	Boltzmann's constant	φ	Free volume

s	Internal variable	w^e	Elastic deformation energy density
$\dot{\varepsilon}_{ref}$	Reference strain-rate	l	Intrinsic material length
l_{el}	Elastic intrinsic material length	G	Shear modulus
E_R	Reduced modulus	H	hardness
κ	Bending curvature	h	Thickness of beam
b	Width of beam	M	Bending moment
M_{nor}	The normalized bending moment	D	Elastic bending stiffness
M_{non}	Non-dimensional bending moment	ΔM_{non}	Difference between non-dimensional bending moments

References

Abdul-Hameed, H., Messager, T., Zaïri, F., Naït-Abdelaziz, M., 2014. Large-strain viscoelastic–viscoplastic constitutive modeling of semi-crystalline polymers and model identification by deterministic/evolutionary approach. Comp. Mater. Sci. 90, 241-252.

Alisafaei, F., Han, C.-S., Garg, N., 2016. On couple-stress elasto-plastic constitutive frameworks for glassy polymers. Int. J. Plast. 77, 30-53.

Alisafaei, F., Han, C.-S., Lakhera, N., 2014. Characterization of indentation size effects in epoxy. Polym. Test. 40, 70-78.

Alisafaei, F., Han, C.-S., Sanei, S.H.R., 2013. On the time and indentation depth dependence of hardness, dissipation and stiffness in polydimethylsiloxane. Polym. Test. 32, 1220-1228.

Anand, L., Ames, N.M., Srivastava, V., Chester, S.A., 2009. A thermo-mechanically coupled

theory for large deformations of amorphous polymers. Part I: Formulation. Int. J. Plast. 25, 1474-1494.

Anand, L., Aslan, O., Chester, S.A., 2012. A large-deformation gradient theory for elastic–plastic materials: Strain softening and regularization of shear bands. Int. J. Plast. 30, 116-143.

Ames, N.M., Srivastava, V., Chester, S.A., Anand, L., 2009. A thermo-mechanically coupled theory for large deformations of amorphous polymers. Part II: Applications. Int. J. Plast. 25, 1495-1539.

Briscoe, B.J., Fiori, L., Pelillo E., 1998. Nano-indentation of polymeric surfaces. J. Phys. D: Appl. Phys. 31, 2395-2405.

Chong, A.C.M., Lam, D.C.C., 1999. Strain gradient plasticity effect in indentation hardness of polymers. J. Mater. Res. 14, 4103-4110.

Díez-Pascual, A.M., Gómez-Fatou, M.A., Ania, F., Flores, A., 2015. Nanoindentation in polymer nanocomposites. Prog. Mater. Sci. 67, 1-94.

Deng, Y., Yi, P., Peng, L., Lai, X., Lin, Z., 2015. Flow behavior of polymers during the roll-to-roll hot embossing process. J. Micromech. Microeng. 25, 065004.

Drozdov, A.D., 2010. Time-dependent response of polypropylene after strain reversal. Int. J. Solids Struct. 47, 3221-3233.

Fleck, N., Hutchinson, J., 1993. A phenomenological theory for strain gradient effects in plasticity. J. Mech. Phys. Solids 41, 1825-1857.

Fu, M., Chan, W., 2011. Geometry and grain size effects on the fracture behavior of sheet metal in micro-scale plastic deformation. Mater. Design 32, 4738-4746.

Ghosh, S., Kumar, A., Sundararaghavan, V., Waas, A.M., 2013. Non-local modeling of epoxy using an a tomistically-informed kernel. Int. J. Solids Struct. 50, 2837-2845.

Han, C.S., Sanei, S.H., Alisafaei, F., 2016. On the origin of indentation size effects and depth dependent mechanical properties of elastic polymers. J. Polym. Eng. 36, 103-111.

Haouala, S., Doghri, I., 2015. Modeling and algorithms for two-scale time homogenization of viscoelastic-viscoplastic solids under large numbers of cycles. Int. J. Plast. 70, 98-125.

He, J.Y., Zhang, Z.L., Midttun, M., Fonnum, G., Modahl, G.L., Kristiansen, H., Redford, K., 2008. Size effect on mechanical properties of micron-sized PS-DVB polymer particles. Polymer, 49, 3993-3999.

Lam, D.C.C., Chong, A., 1999. Indentation model and strain gradient plasticity law for glassy polymers. J. Mater. Res. 14, 3784-3788.

Lam, D.C.C., Keung, L., Tong, P., 2010. Size-Dependent Behavior of Macromolecular solids II: Higher-Order Viscoelastic Theory and Experiments. CMES 66, 73-99.

Lam, D.C.C., Yang, F., Chong, A.C.M., Wang, J., Tong, P., 2003. Experiments and theory in strain gradient elasticity. J. Mech. Phys. Solids 51, 1477-1508.

Lebensohn, R.A., Kanjarla, A.K., Eisenlohr, P., 2012. An elasto-viscoplastic formulation based on fast Fourier transforms for the prediction of micromechanical fields in polycrystalline materials. Int. J. Plast. 32–33, 59-69.

Li, H.Z., Dong, X.H., Wang, Q., Shen, Y., Diehl, A., Hagenah, H., Engel, U., Merklein, M., 2011. Determination of material intrinsic length and strain gradient hardening in microbending process. Int. J. Solids Struct. 48, 163-174.

McFarland, A.W., Colton, J.S., 2005. Role of material microstructure in plate stiffness with

relevance to microcantilever sensors. J. Micromech. Microeng. 15, 1060.

Menčík, J., He, L.H., Němeček, J., 2011. Characterization of viscoelastic-plastic properties of solid polymers by instrumented indentation. Polym. Test. 30, 101-109.

Meng, B., Fu, M., 2015. Size effect on deformation behavior and ductile fracture in microforming of pure copper sheets considering free surface roughening. Mater. Design 83, 400-412.

Nikolov, S., Han, C.S., Raabe, D., 2007. On the origin of size effects in small-strain elasticity of solid polymers. Int. J. Solids Struct. 44, 1582-1592.

Park, S.K., Gao, X.L., 2006. Bernoulli-Euler beam model based on a modified couple stress theory. J. Micromech. Microeng. 16, 2355-2359.

Peng, L., Hu, P., Lai, X., Mei, D., Ni, J., 2009. Investigation of micro/meso sheet soft punch stamping process–simulation and experiments. Mater. Design 30, 783-790.

Poulain, X., Benzerga, A., Goldberg, R., 2014. Finite-strain elasto-viscoplastic behavior of an epoxy resin: Experiments and modeling in the glassy regime. Int. J. Plast. 62, 138-161.

Ran, J., Fu, M., Chan, W., 2013. The influence of size effect on the ductile fracture in micro-scaled plastic deformation. Int. J. Plast. 41, 65-81.

Ree, T., Eyring, H., 1955. Theory of non‐Newtonian flow. I. Solid plastic system. J. Appl. Phys. 26, 793-800.

Shirazi, R.N., Rochev, Y., McHugh, P., 2016. Nanoindentation of solvent-cast and compression-moulded poly (lactic-co-glycolic acid) to determine elastic modulus and hardness. Polym. Test. 50, 111-118.

Spathis, G., Kontou, E., 2004. Nonlinear viscoelastic model for the prediction of double

yielding in a linear low‐density polyethylene film. J. Appl. Polym. Sci. 91, 3519-3527.

Srivastava, V., Chester, S.A., Ames, N.M., Anand, L., 2010. A thermo-mechanically-coupled large-deformation theory for amorphous polymers in a temperature range which spans their glass transition. Int. J. Plast. 26, 1138-1182.

Stölken, J., Evans, A., 1998. A microbend test method for measuring the plasticity length scale. Acta Mater. 46, 5109-5115.

Suzuki, K., Matsuki, Y., Masaki, K., Sato, M., Kuroda, M., 2009. Tensile and microbend tests of pure aluminum foils with different thicknesses. Mat. Sci. Eng. A 513, 77-82.

Swaddiwudhipong, S., Poh, L.H., Hua, J., Liu, Z.S., Tho, K.K., 2005. Modeling nano-indentation tests of glassy polymers using finite elements with strain gradient plasticity. Mat. Sci. Eng. A 404, 179-187.

Tatiraju, R.V.S., Han C.S., Nikolov, S., 2008. Size dependent hardness of polyamide/imide. Open Mech. J. 2, 89-92.

Tjernlund, J.A., Gamstedt, E.K., Xu, Z.-H., 2004. Influence of molecular weight on strain-gradient yielding in polystyrene. Polym. Eng. Sci. 44, 1987-1997.

Treloar, L.R.G., 1975. The physics of rubber elasticity. Oxford university press.

Voyiadjis, G.Z., Shojaei, A., Mozaffari, N., 2014. Strain gradient plasticity for amorphous and crystalline polymers with application to micro-and nano-scale deformation analysis. Polymer 55, 4182-4198.

Wang, J., Yi, P., Deng, Y., Peng, L., Lai, X., Ni, J., 2015. Mechanism of forming defects in roll-to-roll hot embossing of micro-pyramid arrays: II. Numerical study. J. Micromech. Microeng. 25, 115030.

Wang, S., Yang, Y., Zhou, L.M., Mai, Y.M., 2012. Size effect in microcompression of epoxy micropillars. J. Mater. Sci. 47, 6047-6055.

Wei, W., Lam, D.C.C., 2010. Size-Dependent Behavior of Macromolecular Solids I: Molecular Origin of the Size Effect. CMES 64, 213-226.

Wrucke, A.J., Han, C.-S., Majumdar, P., 2013. Indentation size effect of multiple orders of magnitude in polydimethylsiloxane. J. Appl. Polym. Sci. 128, 258-264.

Xu, Z., Peng, L., Fu, M., Lai, X., 2015. Size effect affected formability of sheet metals in micro/meso scale plastic deformation: experiment and modeling. Int. J. Plast. 68, 34-54.

Yang, F., Chong, A.C.M., Lam, D.C.C., Tong, P., 2002. Couple stress based strain gradient theory for elasticity. Int. J. Solids Struct. 39, 2731-2743.

Yoon, W., Huang, X., 2011. A nonlinear viscoelastic–viscoplastic constitutive model for ionomer membranes in polymer electrolyte membrane fuel cells. J. Power Sources 196, 3933-3941.

Zaïri, F., Naït-Abdelaziz, M., Gloaguen, J.-M., Lefebvre, J.-M., 2008. Modelling of the elasto-viscoplastic damage behaviour of glassy polymers. Int. J. Plast. 24, 945-965.

Zhang, P., To, A.C., 2016. Transversely isotropic hyperelastic-viscoplastic model for glassy polymers with application to additive manufactured photopolymers. Int. J. Plast. 80, 56-74.